



# Photodegradation of steroid hormone micropollutants with palladium-porphyrin coated porous PTFE of varied morphological and optical properties

Minh N. Nguyen<sup>a</sup>, Andrey Turshatov<sup>b</sup>, Bryce S. Richards<sup>b</sup>, Andrea I. Schäfer<sup>a,\*</sup>

<sup>a</sup> Institute for Advanced Membrane Technology (IAMT), Karlsruhe Institute of Technology (KIT), Hermann-von-Helmholtz-Platz 1, 76344 Eggenstein-Leopoldshafen, Germany

<sup>b</sup> Institute of Microstructure Technology (IMT), Karlsruhe Institute of Technology (KIT), Hermann-von-Helmholtz-Platz 1, 76344 Eggenstein-Leopoldshafen, Germany

## ARTICLE INFO

### Keywords:

Photosensitiser catalyst  
Collision theory  
Reactive oxygen species  
Physico-chemical water treatment  
PFAS release  
Microreactor

## ABSTRACT

In flow-through reactors, the photodegradation rate can be improved by enhancing contact and increasing the photocatalyst loading. Both can be attained with a higher surface-to-volume ratio. While previous studies focused on thin membranes (30 – 130  $\mu\text{m}$ ) with small pore sizes of 20 – 650 nm, this work employed poly(tetrafluoroethylene) (PTFE) supports, of which pore sizes are in the order of 10  $\mu\text{m}$ , while the porosities and thicknesses are variable (22.5 – 45.3 % and 0.2 – 3 mm, respectively). These porous materials were anticipated to allow a higher loading of porphyrin photosensitisers and better light penetration for subsequent photodegradation of steroid hormone micropollutants via singlet oxygen ( $^1\text{O}_2$ ) generation. The reactor surface refers to the surface within the PTFE pores, while the reactor volume is the total void space inside these pores. The surface-to-volume ratios between  $10^5$  and  $10^6$   $\text{m}^2/\text{m}^3$  are higher than those of typical microreactors ( $10^3$  to  $10^4$   $\text{m}^2/\text{m}^3$ ). The weighted average light transmittance varied from 38 % with the thinnest and most porous support to 4.8 % with the thickest support. Good light penetration combined with minimal absorption by PTFE enhanced the light utilisation of the porphyrins when coated in the porous supports.

Changes in the support porosity of the coated supports minimally affected steroid hormone removal, because the collision frequency in the very large pores remained relatively constant. However, varying the support thickness, porphyrin loading (0.3 – 7.7  $\mu\text{mol/g}$ ), and water flux (150 – 3000  $\text{L}/\text{m}^2\cdot\text{h}$ ), hence the resulting hydraulic residence time, influenced the collision frequency and steroid hormone removal. Results showed that the supports did not outperform membranes most likely because the larger pore size in the former limited contact between the hormones and  $^1\text{O}_2$ .

From photostability testing of the pristine supports, perfluoroalkyl substances (PFAS) released from the supports were found at 10 – 300 ng/L concentrations during accelerated ageing. While PFAS formation was detectable, the quantities during water treatment operations would be extremely low. In summary, this study elucidates the capability and limitations of porous supports coated with photosensitisers to remove waterborne micropollutants.

## 1. Introduction

### 1.1. Occurrence of steroid hormone micropollutants in water

Endocrine-disrupting steroid hormone micropollutants, such as estrone (E1), 17 $\beta$ -estradiol (E2), and 17 $\alpha$ -ethinylestradiol (EE2), induce high risks of reproductive disorders in living organisms (Lauretta et al., 2019; Vandenberg et al., 2012) and deserve global attention (Johnson

et al., 2020; Yang et al., 2022). Due to the endocrine-disrupting effects of steroid hormones at extremely low concentrations, of several nanograms per litre (Arlos et al., 2018), the European Union (EU) proposed strict limits for these micropollutants in both drinking and surface waters. For drinking water, the limit for E2 has been set to 1 ng/L (European Commission, 2022a), while for surface water, the limits for E1, E2, and EE2 are fixed at 0.36, 0.18, and 0.017 ng/L, respectively (European Commission, 2022b). In wastewater effluents and surface water, the

\* Corresponding author at: Karlsruhe Institute of Technology (KIT), Hermann-von-Helmholtz-Platz 1, 76344 Eggenstein-Leopoldshafen, Germany.  
E-mail address: [Andrea.Iris.Schaefer@kit.edu](mailto:Andrea.Iris.Schaefer@kit.edu) (A.I. Schäfer).

<https://doi.org/10.1016/j.watres.2024.123034>

Received 23 October 2024; Received in revised form 10 December 2024; Accepted 21 December 2024

Available online 22 December 2024

0043-1354/© 2024 The Authors. Published by Elsevier Ltd. This is an open access article under the CC BY license (<http://creativecommons.org/licenses/by/4.0/>).

steroid hormone micropollutants may occur at much higher concentrations than the limits (up to 106 and 25 ng/L, respectively) (Ciślak et al., 2023; Tang et al., 2020; Tran et al., 2018). The near-complete removal of steroid hormone micropollutants requires advanced treatment technologies (such as adsorption, filtration, and/or oxidation) at the tertiary or quaternary water treatment stages (Abily et al., 2023; United Nations, 2017).

### 1.2. Elimination of micropollutant in flow-through photocatalytic reactors

Photocatalytic oxidation is a technology capable of eliminating recalcitrant micropollutants, including steroid hormones (Orozco-Hernández et al., 2019; Su et al., 2024; Wang et al., 2020). To achieve high-throughput operation, a number of flow-through photocatalytic reactors have been developed by integrating porous supports or membranes with photocatalytic processes, in which micropollutants are degraded and continuously replenished (Alvey et al., 2023; Kumari et al., 2020; Ly et al., 2023; Mozia, 2010). Photocatalysts or photosensitisers (PS) can be immobilised on the entire surface area of the flow-through reactor – not only the exposed outer surfaces but also the inner walls of the porous supports or membrane pores. This approach enables compact, modular designs while minimising the risk of photocatalyst washout and aggregation (Hodges et al., 2018; Qing et al., 2020).

The photocatalysts or photosensitisers (PS) can be deposited onto the surface of the pores when the PS sizes are smaller than the pore sizes. Such nanoscale coatings – whether comprised of nanoscale particles anchored onto the substrate (Fischer et al., 2015), conformal thin films of inorganic photocatalysts (Berger et al., 2020), or organic PS (Lyubimenko et al., 2019) – can allow light to penetrate deeper into the porous materials. As a result, photons can be utilised by the photocatalysts/PS in greater depths (Nyamutswa et al., 2020). Nevertheless, these flow-through reactors with immobilised photocatalysts/PS have several drawbacks. Firstly, the quantity of photocatalysts or PS is limited and depends on the amount of internal pore surface (Cambié et al., 2016; Hodges et al., 2018). Secondly, even though the mass transfer of micropollutants is vastly improved in the pores, it is still a limitation within very short hydraulic residence times (HRTs) due to the small reactor volume compared to the batch systems (Chen et al., 2000; Hodges et al., 2018). This mass transfer limitation reduces the number of effective collisions between reactive oxygen species (ROS) and target compounds in the aqueous phase, hindering overall process efficiency (Lyubimenko et al., 2022b; Nguyen et al., 2024). Overcoming the mass transfer limitation warrants further in-depth investigation.

### 1.3. Mass transfer limitation with photocatalysts immobilised in the substrate pores

One strategy to mitigate mass transfer limitations is by increasing the surface-to-volume ( $S/V$ ) ratio of the reactor. Smaller volumes (and usually smaller pore diameters) of the reactor channels/pores are associated with shorter distances and thus time required for ‘mixing’, *i.e.* the diffusion of target micropollutants from the pore centre towards the pore surface (Cambié et al., 2016). A larger internal surface allows a higher quantity of photocatalysts to be immobilised (Chen et al., 2022). High  $S/V$  ratios can be achieved by decreasing the pore width or pore diameter at a given porosity. Microreactors with channels/pore widths of several hundred micrometres (Fig. 1 A) afford  $S/V$  ratios in the order of  $10^3 - 10^4 \text{ m}^2/\text{m}^3$  (Gorges et al., 2004; Li et al., 2018), which is higher than slurry reactors and other conventional types ( $S/V = 10^1 - 10^3 \text{ m}^2/\text{m}^3$ ) (Gorges et al., 2004; Su et al., 2014). The  $S/V$  ratios of photocatalytic microporous media (Fig. 1 B) fall between those of microreactors and photocatalytic membrane reactors (PCMs). PCMs with micro- and ultrafiltration membrane substrates (Fig. 1 C) have greatly enhanced  $S/V$  ratios in the range of  $10^6 - 10^8 \text{ m}^2/\text{m}^3$ . Mass transfer limitations are eliminated almost completely in PCMs with

nanofiltration membrane substrates, where the  $S/V$  ratio is in the range of  $10^{10} \text{ m}^2/\text{m}^3$  (Fig. 1 D). In such PCMs, the micropollutants are in good contact with the PCM pore walls, predominantly due to the nanoscale pore sizes (tens to hundreds of nanometres). Inside reactors with moderate or low  $S/V$  ratios, the micropollutants can be photodegraded in the liquid phase by ROS diffusing from the photocatalyst/PS surface (Fig. 1 E), for instance, singlet oxygen ( $^1\text{O}_2$ ) generated from dissolved oxygen via a type II energy transfer process at the porphyrin PS (Fig. 1 F) (Baptista et al., 2017; Dumoulin, 2012).

Higher  $S/V$  ratios of flow-through photocatalytic reactors have been found to correlate with better photodegradation of pollutants (yellow bar in Fig. 1). For example, Regmi et al. (2020) reported that the removal of methylene blue (as an indicator) using microfiltration substrates with a photocatalytic titanium dioxide ( $\text{TiO}_2$ ) coating is 30 – 65 % in flow-through mode (*i.e.* solution flow was through the  $\text{TiO}_2$ -coated pores;  $S/V \sim 10^6 \text{ m}^2/\text{m}^3$ ) depending on light intensity. In contrast, methylene blue removal remained consistently low (<10 %) in flow-along mode, where the solution flow was parallel to the PCM surface in a microreactor channel ( $S/V = 1.4 \cdot 10^3 \text{ m}^2/\text{m}^3$ ). In another study with porphyrin-coated PCMs, Lyubimenko et al. (2022b) achieved an improvement in E2 removal at low porphyrin loadings from 10 to 82 % by decreasing the average pore diameter from 200 to 20 nm (hence the  $S/V$  ratio increased from  $7.1 \cdot 10^6$  to  $4.3 \cdot 10^7 \text{ m}^2/\text{m}^3$ ). Improved pollutant removal was correlated with faster photodegradation kinetics due to enhanced mass transfer.

### 1.4. Light penetration inside the photocatalytic substrates

In addition to mass transfer, light penetration in the photocatalytic reactors, which is related to the geometry and optical properties of the membrane/support, can be a limitation and needs to be enhanced. The higher the light scattering, the stronger the attenuation of light intensity with penetration depth, likely limiting light – especially at shorter wavelengths – from reaching the photocatalysts or PS located deep within the porous substrates where ROS are generated.

Several optical properties can affect the light scattering and distribution. Firstly, it should be noted that nanoscale features do not scatter light in the same manner as microscale features. When the pore sizes have dimensions that are much greater than the wavelengths of visible light (*e.g.* in the order of 10  $\mu\text{m}$ ), light of all wavelengths will be scattered equally. This phenomenon is referred to as Mie scattering. In contrast, when the pore diameters are smaller than the wavelengths of light (*e.g.* 100 nm), the pores preferentially scatter shorter wavelengths, such as blue light. This phenomenon is known as Rayleigh scattering (Lockwood, 2016). Conversely, light of longer wavelengths will penetrate these small pores more deeply, some even being transmitted through the substrate. Secondly, the scattering efficiency decreases significantly for smaller pore sizes, meaning that substrates with smaller pores appear less bright white (Yu et al., 2023). This effect is further pronounced when the difference in refractive index between the substrate material and the intervening void (air or water, depending on whether the substrate is dry or wet) is reduced (Lockwood, 2016). In nanoscale coating layers, where thicknesses are much smaller than the wavelengths of visible light, the light only recognises an ‘effective medium approximation’ with a single effective refractive index instead of separate layers at the surface with different refractive indices (such as the substrate surface and the coating) (Bruggeman, 1935). Hence, the thicker the coating layer (or the higher photocatalyst/PS loading) with a high refractive index, the higher the effective refractive index of the combined substrate and coating, and hence the stronger light scattering. Thirdly, both the thickness of the porous substrates and their porosity will affect the amount of light scattered and transmitted. Penttilä and Lumme (2009) determined that for the microporous substrates, a broad maximum in the brightness of reflected scattering existed around 40 – 60 % porosity, while, for nanoporous media, the brightness of reflected scattering steadily declines with increasing porosity. Finally, the

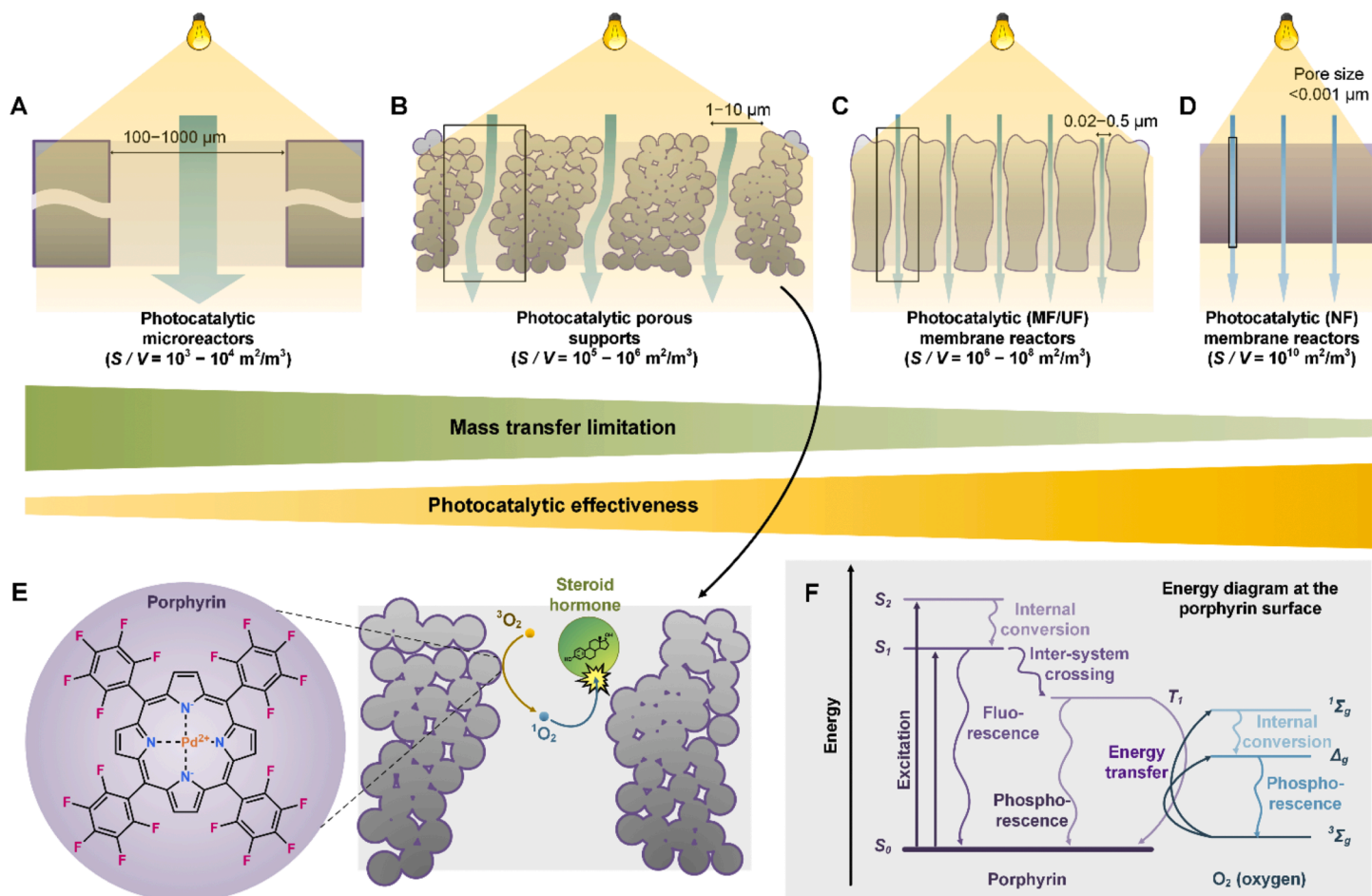


**Fig. 1.** A to D – Schematic views of photocatalytic microreactors (A), porous supports (B), micro-/ultrafiltration (MF/UF) membrane reactors (C), and nanofiltration (NF) membrane reactors (D) with the corresponding surface-to-volume ( $S / V$ ) ratios. Black hollow boxes indicate single reactor channels with reactor volume in the order of  $A > B > C > D$ . Photocatalysts (or photosensitisers) are immobilised on the reactor (pore) wall. The green and yellow bars highlight the trends in mass transfer limitation (higher in larger-dimension reactors) and photocatalytic effectiveness (higher in smaller-dimension reactors), respectively. E – schematic of the conversion from dissolved oxygen to singlet oxygen, which is the ROS for steroid hormone degradation, at the surface of photosensitisers (*i.e.* palladium porphyrin) coated onto the porous support. F – Energy diagram highlighting the type II energy transfer process at the photosensitiser surface.

morphology plays an important role and that even modern simulations need to assume that particle/pore shapes are spherical (Han et al., 2014), which is often not the case in reality. The randomness and high tortuosity of pores hinder light transmission and promote scattering (Ramirez-Cuevas et al., 2022).

### 1.5. Quantification of mass transfer and light penetration limitations with the collision theory

To quantify the impacts of both mass transfer and light penetration on photodegradation performance, Nguyen et al. (2024) adapted the collision theory framework (Smoluchowski, 1917) to calculate the degradation rate in porphyrin-coated PCMs. This framework applies to reaction systems where reactants have extremely high reactivity for each other; as such, the reaction rate is solely limited by mass transfer (i.e. the diffusion of reactants until the collision). The prerequisites for this calculation are the molar concentrations and diffusivities of  $^1\text{O}_2$  ROS and steroid hormone micropollutants in the liquid phase. The concentration of  $^1\text{O}_2$  depends on its lifetime, the absorbed photon flux, and the photon conversion capacity (or the quantum yield of  $^1\text{O}_2$  generation) of the photosensitiser (Lyubimenko et al., 2021; Wilkinson et al., 1995). In the study by Nguyen et al. (2024), the average pore diameter of the PCM was 200 nm, which is sufficiently small to facilitate the diffusion of  $^1\text{O}_2$  to most pore spaces within its lifetime of approximately 3  $\mu\text{s}$ . The average diffusion distance for this lifetime is about 270 nm in water (Skovsen et al., 2005) and thus the same order of magnitude as the pore diameter. The collision theory can potentially be applied in smaller pores down to  $\sim 10 - 20$  nm, but calculations may deviate in  $<10$  nm pores as the mass transfer behaviours of solutes are strongly influenced by pore wall interactions (Tang et al., 2024; Thiruraman et al., 2020). In larger pores (e.g. micropores with sizes of 1 – 100  $\mu\text{m}$ ), such as the porous support materials used in this work, the collision theory can be applied, even though  $^1\text{O}_2$  will not be present in a large amount of pore spaces for collision with the target micropollutants.

### 1.6. Photodegradation with poly(tetrafluoroethylene) (PTFE) photocatalytic supports

Porous poly(tetrafluoroethylene) (PTFE) material exhibits good resistance to heat, chemicals, and ultraviolet (UV) light (Chin et al., 2006; Dhanumalayan and Joshi, 2018), and can be processed into membranes or porous supports by stretching, sintering, and electrospinning (Guo et al., 2022). Owing to the stability and commercial availability of PTFE, the material is widely used in gas filtration, membrane distillation (Guo et al., 2022; Huang et al., 2013), and as catalyst substrates for pollutant degradation (Huang et al., 2012; Qin et al., 2020). PTFE supports absorb nearly no light in the UV (250 – 400 nm) and visible regimes (400 – 700 nm) (Araujo et al., 2019; Quill et al., 2020), hence the parasitic optical absorption is minimal. Depending on the thickness and pore size/porosity, PTFE substrates can achieve varied degrees of light scattering and transmission. For instance, semi-transparent porous PTFE substrates are utilised in algal cultivation chambers, where light transmission and efficient gas exchange through these substrates promote the growth of algae (Nowack et al., 2005). When placed in water, PTFE membranes have been reported to become nearly transparent (Nguyen et al., 2024). This phenomenon is due to the difference in refractive index ( $\Delta n$ ), which is the governing factor behind scattering phenomena of PTFE ( $n = 1.33 - 1.39$ ) (Gauch et al., 2013) and water ( $n = 1.33$ ) approaches zero. By coating with photoactive species,  $\Delta n$  and hence light scattering – at wavelengths outside the absorption bands of the coating species – in the pores can be further enhanced. Several types of photocatalysts or PS in the coating layer have significantly higher refractive indices than PTFE; for instance, palladium-porphyrins have a refractive index ranging from 1.5 to 3.0 (Morisue et al., 2023), while  $\text{TiO}_2$  exhibits a refractive index between 2.0 and 2.7 (Richards, 2004). At the absorption wavelengths, the coated

photocatalyst/PS suppresses the light reflectivity of the surface and acts as a sacrificial light-absorbing material (Hussein et al., 2002).

### 1.7. Toxicological concerns over the use of fluorinated polymer supports

PTFE is a favoured substrate for photocatalytic membranes due to its high chemical stability. During extended exposure to UV light, the possibility of several polymer chains being broken cannot be ruled out (Raota et al., 2023). When the incident photon energy from irradiation exceeds the bond dissociation energy of the polymer backbone (e.g. C – C bonds in PTFE), these bonds become susceptible to breaking, leading to a chain reaction (Andrady, 1996; Singh and Sharma, 2008). This process can cause the formation of per- and polyfluoroalkyl substances (PFAS). Chain scission of fluoropolymers and PFAS formation has been reported as possible under exposure to strong UV light, for example, exposure for 4 h under 222 nm UV at a dose of  $2 \cdot 10^{18}$  photons/Ls (Xin et al., 2023). In contrast, the C – F bonds in PTFE are very strong, likely remaining unbroken by oxidation with UV light and ROS (Gar Alalm and Boffito, 2022). Therefore, reduction may be a more viable pathway to achieving defluorination (Bentel et al., 2019; Calvillo Solís et al., 2024; Ren et al., 2021).

PFAS have been linked to kidney damage, disorders of the endocrine and reproductive systems, impairment of immune functions, and increased risk of cancer (Bell et al., 2021; Blake et al., 2018; Kvaalem et al., 2020; Wielsøe et al., 2015). The EU regulates the concentrations of total PFAS and the sum of several priority PFAS in drinking water to a maximum of 500 and 100 ng/L, respectively (European Parliament and Council, 2020). Additionally, an EU Directive proposal suggests a threshold of 4.4 ng/L for total PFAS in surface water (European Commission, 2022b). Significantly higher concentrations of various PFAS, ranging from sub- to several micrograms per litre, have been detected in waters downstream from fluoropolymer manufacturing sites (Joerss et al., 2022; Newton et al., 2017; Pétré et al., 2022). In response to the risks of PFAS release, the EU plans to phase out PTFE and other fluoropolymers in the near future (European Chemicals Agency ECHA, 2023). This will pose challenges for the availability of chemically stable polymeric substrates for photocatalytic reactors.

In this study, the steroid hormone photodegradation performance of fifteen porphyrin-coated microporous supports with varied thicknesses and porosities was evaluated. Compared to UF/MF membranes with narrower pores, the porous supports can be fabricated more easily, and, because of the lower flow resistances, are available with greater thicknesses (up to several millimetres, for instance). Hence, these porous supports are an interesting option as photocatalytic substrates. The limiting mass transfer and light penetration in these supports will be examined via the collision theory framework previously developed for ultra-thin PCMs with sub-nanometre pores (Nguyen et al., 2024).

The novelty of this research lies in the application of collision theory to micropores to better understand photocatalytic process limitations for materials with larger pores and higher thicknesses than membrane substrates. PFAS leaching measurements under exposure to intense ( $2223 \text{ W/m}^2$ ) UV/violet light for 250 h are performed to evaluate possible release. The specific research questions are; i) What are the optical properties of PTFE supports as a function of porosity and layer thickness? ii) How does photodegradation of steroid hormones depend on support morphology, porphyrin loading, and flux? and iii) What is the extent of PFAS leaching when PTFE supports are exposed to simulated terrestrial sunlight?

## 2. Materials and methods

### 2.1. Filtration system and protocol for photocatalytic experiments

The experiments were performed using a photocatalytic membrane system adapted from a previous study (Lyubimenko et al., 2022b). The key difference is that to accommodate the thick (1 – 3 mm) PTFE

support coupons, an alternative membrane cell containing a 'well' with a total depth of 3.7 mm (channel depth 0.7 mm and well depth 3 mm) was used. For support coupons with thicknesses of 0.2 – 0.4 mm, the same cell as reported by Lyubimenko et al. (2022b) was employed. A quartz glass window allows the illumination of the photocatalytic supports inside either of the membrane cells. A solar simulator (SolSim SINUS-70, WaveLabs, Germany) was used as the source of simulated terrestrial sunlight (wavelength range 350 – 1150 nm) at a light intensity of 14 mW/cm<sup>2</sup> (Fig. S1). The maximum intensity of the output spectrum (350 – 1150 nm) is 81.5 mW/cm<sup>2</sup>, corresponding to a fraction of the reference AM1.5 g solar spectrum (280 – 4000 nm) (ASTM, 2012) with an intensity of 100 mW/cm<sup>2</sup>.

The schematic of the filtration system is illustrated in Fig. 2. The feed flow rate in the range from 0.5 to 10 mL/min was controlled by a high-pressure dosing pump (HPLC Blue Shadow 80P, Knauer, Germany). Feed temperature control at 24.0 ± 0.5 °C was achieved with a water chiller (Minichiller 300 OLÉ, Huber Kältemaschinenbau, Germany) connected to the water-jacketed feed bottle (1 L volume). A LabView program (National Instruments, USA) allowed system control and experimental data acquisition.

Experiments were performed following a previously revised filtration protocol for photocatalytic membranes (Nguyen et al., 2024) (Table S1), which consists of the following steps: i) conditioning of the support, ii) permeability measurement, iii) main photocatalytic experiment with 100 mL dark phase and subsequent 600 mL light phase, iv) another permeability measurement, this time after the photocatalytic experiment, and v) dismantling of the support and system cleaning. The ambient conditions (room temperature and humidity) were recorded and given in Fig. S2 A and B.

Previous work demonstrated that steroid hormone removal by the porphyrin-coated substrates remained consistent during 158 h of exposure to a light intensity that was 3.2 times lower than the light intensity used in this study (Lyubimenko et al., 2021). It is implied that the degradation of porphyrins (if any) would not impact the steroid hormone photodegradation performance in experiments that lasted up to 24 h.

## 2.2. Pristine PTFE supports

Commercial PTFE porous support materials (Berghof Fluoroplastic Technology GmbH, Germany) produced via a sintering process at 300 °C

(Berghof GmbH, 2024) were used. The 15 different support types have various thicknesses (0.2 – 3 mm) and porosities (22.5 – 45.3 %), as shown in Table S2. The surface and cross-sectional micrographs of the supports (Fig. S3 – S6) do not reveal significant morphological differences, as the range of porosities remains relatively narrow. The pure water permeabilities were determined from the slope of flux vs. pressure (Fig. S7), and varied from 1,760 to 64,200 L/m<sup>2</sup>.h.bar. Both the internal surface area and pore volume increased with increasing support thickness; the *S/V* ratio of all the supports varied within the range of (2.3 – 6.1) · 10<sup>5</sup> m<sup>2</sup>/m<sup>3</sup> (Table S2 and Fig. S8). From the *S/V* ratio, the average pore diameters of the supports (with the assumption that the pores are uniform and cylindrical) fall between 7.6 and 17 μm, which are larger than the wavelengths of visible light.

## 2.3. Coating of the PTFE supports with porphyrins

The PTFE supports were coated with 5,10,15,20-tetrakis(pentafluorophenyl)-21H,23H-porphine palladium(II) (PdTFPP, >94 %, Frontier Scientific, USA) to form photocatalytic PdTFPP-PTFE supports via a process described elsewhere (Lyubimenko et al., 2019). Briefly, the support coupons were rinsed in acetone (99 %, Merck Millipore, USA) and methanol (>99 %, Merck Millipore, USA) in an ultrasonic bath (USC 300 T, VWR, USA) and transferred to a stainless-steel shaker plate. Then, a 1.5 mL aliquot of 13.9 ± 0.5 mM PdTFPP solution in tetrahydrofuran (THF, 99.9 %, Merck Millipore, USA) was added to the plate, and the plate was shaken for 4 h on a mini-shaker (Shaker KM-2, Edmund Büchler, Germany). The coated supports were cleaned with water and stored in Milli-Q water to avoid de-wetting (Lyubimenko et al., 2019).

The PdTFPP loading was determined via the washing method as described in a previous study (Nguyen et al., 2024). In brief, the PdTFPP-PTFE supports were submerged three times in a fixed volume of THF (10 mL each time). The absorbance of the washing solution was then determined, and the PdTFPP concentration was calculated from the concentration – absorbance linear relationship. Based on this concentration, the mass of PdTFPP released from washing and the porphyrin loading were then calculated. The porphyrin loading (equal to the molar mass of porphyrin divided by the mass of the support) was reported in Table S3. The PdTFPP loading increased from 3 to 8 μmol/g with increasing support porosity from 22.5 to 45.3 % (Fig. S9). The loading was independent of the support thickness in the range of 0.2 – 3 mm;

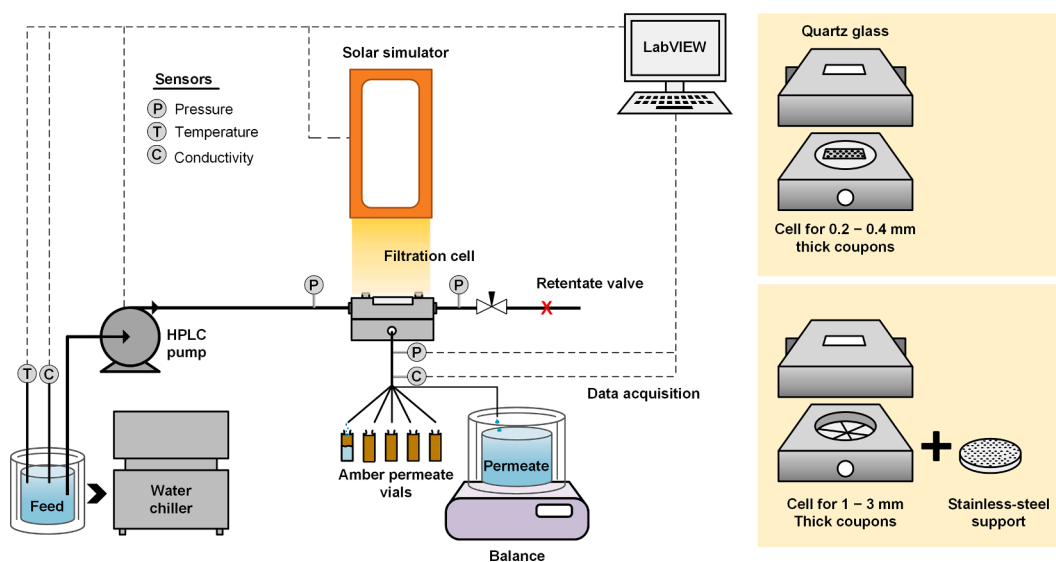


Fig. 2. Photocatalytic membrane system with high-pressure dosing pump, photocatalytic filtration cell (two types), switching valve to separate permeate samples, balance to collect permeate for flux measurements, number of pressure (P), temperature (T), and electrical conductivity (C) sensors, and water chiller to control the feed temperature.

however, the molar mass of porphyrins scaled with the thickness and mass of support (Fig. S10). The porphyrin loading before and after the photocatalytic experiment did not vary significantly (for instance,  $5.1 \pm 0.6$  vs.  $4.9 \pm 0.6$   $\mu\text{mol/g}$  for the thin coated coupons with a porosity of 30.4 % and thickness of 0.2 mm), implying that PdTFPP leakage was insignificant.

To vary the PdTFPP loading in a particular support, a different concentration of PdTFPP in the THF coating solution was prepared, instead of  $13.9 \pm 0.5$  mM. The relationship between the loading and PdTFPP concentration in the coating solution is given in Fig. S11.

#### 2.4. Surface and morphological characterisation of pristine supports

Scanning electron microscopy (SEM) was performed with a SUPRA 60VP (Carl Zeiss AG, Germany) to characterise the morphology of the support surface and cross-section. A fixed acceleration voltage of 5 keV was deployed, and secondary electrons were detected with an Everhart – Thornley Secondary Electron Detector. For cross-sectional analysis, the support pieces were cut at  $-30$  °C with a microtome (Leica CM1860 UV, Leica Biosystems, Germany), and then the pieces were submerged in a cryo-sectioning liquid (product code 14020108926, also supplied by Leica Biosystems). After the cryo-sectioning liquid was frozen, a cross-section was cut with a sharp steel knife. The sample was then taken out at room temperature to melt the sectioning liquid and cleaned with Milli-Q water. All pieces were adhered to carbon tape and sputtered with a 10 nm layer of conductive gold with a sputter coater (SCD 005, BAL-TEC, Germany) and characterised in SEM under magnification levels between 70 and 10,000.

Nitrogen gas adsorption and desorption isotherm experiments were done with the Quadrasorb EVO instrument (Quantachrome, USA) to determine the surface area of the pristine supports. Approximately 2 g of support fragments were degassed at 373 K in vacuum and analysed at 77 K (the relatively large sample mass compensated for the expected low specific surface area in the order of  $0.1$   $\text{m}^2/\text{g}$ ). The relative vapour pressure was varied between 0.005 and 0.99. Surface analysis was done with the QuadraWin v7.1 software (Quantachrome, USA). The specific surface area was calculated in the relative vapour pressure range of approximately 0.05 – 0.32 according to the multi-point Brunauer-Emmett-Teller model (Brunauer et al., 1938). Three measurements were performed per sample, and the average value was reported. The software also provides a function for calculating the volume of pores that are <100 nm in size. However, the larger pores could not be measured due to the instrument sensitivity; hence, the pore volume analysis was not applicable for the PTFE supports that constitute pores in the several micrometre range.

Fourier transform infrared spectroscopy (FTIR) with attenuated total reflection (ATR) was performed with a Spectrum Two (Perkin Elmer, USA) to determine the chemical composition and structural changes of the pristine supports due to light exposure in accelerated aging. The irradiated 0.2 – 0.4 mm thick supports were dried in air for 24 h. The wavenumber varied from 4000 to  $450$   $\text{cm}^{-1}$  with a resolution of  $1$   $\text{cm}^{-1}$ , and 20 scans were performed per sample.

#### 2.5. Optical characterisation of pristine and porphyrin-coated supports

The absorbance and transmittance spectra of the pristine and coated supports were obtained using a spectrophotometer equipped with an integrating sphere (Cary 7000 Universal Measurement Spectrophotometer, Agilent Technologies, USA) in the wavelength range between 300 and 1200 nm. The measurement procedure is as described elsewhere (Berger et al., 2020). Briefly, the support coupon (2.5 mm diameter) was placed in a water-filled quartz cuvette (40 mm  $\times$  40 mm and light path 10 mm, Starna Scientific, UK). The quartz cuvette was then mounted inside the integrating sphere for measurements of absorbance (which is the percentage of light absorbed by the support, equal to 100 % minus the percentages of scattered and transmitted light detected in the

integrating sphere), and just outside of the integrating sphere for measurements of transmittance (which is the percentage of light transmitted through the support and detected in the integrating sphere). The pristine coupons were pre-soaked in methanol in a glass beaker placed in an ultrasonic bath for 1 h, then rinsed with Milli-Q water and kept submerged in Milli-Q water for the characterisation. The PdTFPP-PTFE supports were already submerged in Milli-Q water following the coating procedure.

#### 2.6. Micropollutants and solution chemistry

Radio-labelled [2,4,6,7- $^3\text{H}$ ] 17 $\beta$ -estradiol (E2), [1,2,6,7- $^3\text{H}$ ] progesterone (P), and [1,2,6,7- $^3\text{H}$ ] testosterone (T) were purchased from PerkinElmer, USA. Radio-labelled [6,7- $^3\text{H}$ ] estrone (E1) was purchased from BioTrend, Germany. All the steroid hormones were supplied as solution in ethanol. The feed solution in photocatalytic experiments contained 100 ng/L individual steroid hormone in a background solution of 1 mM  $\text{NaHCO}_3$  (dissolved from 99.7 % powder, Bernd Kraft, Germany) and 10 mM NaCl (dissolved from 99.9 % powder, VWR, Germany). The natural pH of this background solution was in the range of  $8.2 \pm 0.1$ . pH adjustment was done with 1 M HCl (diluted from 37 % HCl, Carl Roth, Germany) and 1 M NaOH (dissolved from NaOH pellets, analytical-grade (EMSURE), Merck Millipore).

#### 2.7. Water quality analysis

The dissolved oxygen (DO) concentration and pH were monitored in the feed using an external oxygen sensor (FDO-925, WTW, Germany) and pH sensor (pH/Cond 3320, WTW, Germany). Before each measurement, the DO sensor was tested at 100 % air oxygen saturation by inserting in an FDO Check vessel (WTW, Germany), which is a vessel that contains saturated concentration of oxygen in air. A small variation of DO between 8.3 and 9.0 mg/L at ambient room temperature indicates that the electrode was working. The feed pH and DO concentration were then measured before each experiment and recorded in Fig. S2 C and D. Feed electrical conductivity and temperature were recorded using a thermo-coupled conductivity sensor (Blackline CR-GT/-EC/-GS, 202,922, WTW), and permeate electrical conductivity was recorded with an in-line contactless sensor (sensor ET131, eDAQ, France).

The steroid hormone concentrations in the feed and permeate samples were determined using ultra-high performance liquid chromatography (UHPLC, Flexar FX-20, Perkin Elmer, USA) coupled with a flow scintillation analyser (FSA) (Radiomatic 625TR, Perkin Elmer, USA) based on a previously described protocol (Lyubimenko et al., 2020). This analytical protocol was further adapted with a reduced UHPLC pump flow rate (from 0.25 to 0.2 mL/min) to prevent overpressure, a higher injection volume (from 100 to 200  $\mu\text{L}$ ) to increase the peak areas in chromatograms, and a reduced gradient elution time for E1 and E2 to fasten analyses (Nguyen et al., 2024). The detection limit of the revised HPLC-FSA protocol is around 3 – 5 ng/L, which is similar to the detection limit reported with the original protocol, of 3.4 ng/L (Lyubimenko et al., 2020).

Liquid scintillation counting (LSC) was performed with a Tri-Carb 4910 TR instrument (Perkin Elmer, USA) to determine the E2 concentration in the dark phase (in pre-saturation investigation) by quantifying the activity of tritium (Birks, 1975). For each measurement, a mixture of 1 mL of sample and 1 mL of scintillation cocktail (Optiscint LLT, PerkinElmer) was prepared in a 20 mL glass vial. Each measurement was done in triplicate with a counting time of 10 min each, and the average activity value was reported. The activity was correlated to steroid hormone concentration via a calibration with known concentrations of steroid hormones between 0.2 and 100 ng/L. LSC allows higher precision and lower detection limits (0.1 – 0.2 ng/L) compared to UHPLC-FSA. However, LSC is not suitable for quantifying steroid hormones in the permeate samples collected during the light phase, as it cannot separate residual steroid hormones from their breakdown

products. However, LSC can determine the total activity and tritium concentration of all the micropollutant fragments, which is useful to quantify the steroid hormones plus the degradation products adsorbed in the light phase (Liu et al., 2024).

The analysis of twenty-five types of PFAS in accelerated aging samples was performed by a certified laboratory (TZW Karlsruhe, Germany) with high performance liquid chromatography and tandem mass spectrometry (HPLC/MS-MS) after solid-liquid extraction in accordance with standard protocol DIN 38,407–42:2011–03+ (German Institute for Standardisation, 2011). The limit of quantification of the method is 2 ng/L for each PFAS, requiring a large pre-concentrated sample volume of 1 L. Due to the small sample volumes (below 10 mL) in these experiments, the limit of quantification was 10 ng/L for each PFAS. Measurements were not replicated, although from method validation, the resulting uncertainty of micropollutant analyses can be as high as 25 %.

## 2.8. Presaturation of thick supports (2 – 3 mm)

For thicker porous supports with higher surface area, a dark phase duration of 100 mL permeate was not sufficient for the adsorption of steroid hormones to reach saturation. This saturation step is important to maintain a low or negligible concentration gradient of steroid hormones in the radial direction for the application of the collision theory framework (Nguyen et al., 2024). Therefore, these coupons were pre-saturated with steroid hormones in a static adsorption experiment. To pre-saturate the thick supports (2 – 3 mm), a static adsorption experiment was carried out for 26 h with 150 ng/L E2 and support coupon with a diameter of 2.5 cm and an area of 4.91 cm<sup>2</sup>. The protocol was adapted from prior work (Tagliavini et al., 2017). The long residence time of up to 26 h was chosen to ensure that steroid hormones diffuse into the support pores and saturate the adsorption sites. A volume of E2 solution of 100 mL was placed in a 250 mL conical flask in an incubator shaker (temperature set at 23 °C). At time zero, the wetted support was added to the flask, and the shaking speed was then set to 260 rpm. After 1, 3, 5, 7, 9, 24, and 26 h, an aliquot of 0.5 mL was extracted from the flask for analysis. The concentration of 150 ng/L was selected to ensure that, at adsorption equilibrium, the liquid phase concentration would be around 100 ng/L, thus matching the concentration used in the subsequent filtration step. This filtration step is necessary to attain adsorption equilibrium because in static adsorption, steroid hormones did not penetrate all the surface accessible in filtration. A total volume of 700 mL of 100 ng/L hormone was filtered through the support following the filtration protocol but with the light turned off (*i.e.* completely in the dark phase). In both static adsorption and dark-phase filtration experiments, the samples were analysed with LSC, which allows higher accuracy and lower detection limits than the UHPLC-FSA (Imbrogno et al., 2024).

## 2.9. Release of PFAS due to reactive oxygen and UV/violet light exposure

Accelerated aging experiments were performed to examine the photo-stability of support materials and leakage of PFAS upon exposure to UV/violet light inside a photodegradation chamber (Compact UV-LED Chamber BSL-01 ECO+, Opsytec Dr. Grobel, Germany). The total light dose inside the photodegradation chamber in 250 h is equivalent to 5.5 months of continuous operation under simulated sunlight with a light intensity of 14 mW/cm<sup>2</sup> (Lyubimenko et al., 2022a; Raota et al., 2023). The accelerated ageing experiments were done with the pristine (uncoated) supports of varied thicknesses (0.2, 0.3, 0.4, 1, 2, and 3 mm, respectively).

For each ageing experiment, a support coupon (each has a diameter of 2.5 cm and an area of 4.9 cm<sup>2</sup>) was placed in an aluminium tray (base dimension 40 mm · 25 mm) containing 10 mL of Milli-Q water (Milli-Q A+ system, Millipore, USA). The trays were then placed inside the photodegradation chamber. Accelerated ageing was carried out at a total light intensity of 2223 W/m<sup>2</sup> (UV LED: 365 nm, 981 W/m<sup>2</sup> plus

violet LED: 405 nm, 1242 W/m<sup>2</sup>) as described in a previous study (Raota et al., 2023). With a coupon thickness increase from 0.2 to 3 mm, the corresponding UV and violet light doses decrease from 9.0 · 10<sup>21</sup> to 6.0 · 10<sup>20</sup> and from 1.3 · 10<sup>22</sup> to 8.4 · 10<sup>20</sup> photons/L.s, respectively. The reduction in light dose with increasing support thickness is attributed to the larger support volume being irradiated by the same quantity of photons. The base of the photodegradation chamber was modified to accommodate a water-jacketed copper plate that is connected to a water chiller (Minichiller 300, Huber Kaltemaschinenbau). The temperature at the base of the chamber was maintained at approximately 21 °C by setting the chiller to the same temperature. The sample holders were covered by borosilicate glass sheets (Schott BF33, 100 mm · 100 mm · 3.3 mm) to reduce water evaporation. Each glass sheet could cover up to three trays. The cover was not air-tight, leading to partial evaporation. The masses of the sample holder, support coupon, and water before and after accelerated aging experiments were recorded to determine the volume loss due to evaporation. During 250 h accelerated aging experiments, the volume loss was between 40 and 60 %.

After 250 h, each coupon was removed with a stainless-steel tweezer, and the water in the holders was transferred in clean 20 – 25 mL glass vials. A background water sample was extracted from holders without support coupons. The glass vials were covered with clean aluminium foil before they were capped with plastic caps for transfer to avoid plastic contamination. The samples were stored at 4 °C in the fridge until analysis. The concentrations of PFAS species were corrected for the volume loss (by multiplying with the percentage of the remaining volume).

## 2.10. Surface area to volume ratio calculations

The calculations of flux, permeability, removal and rate of disappearance are provided in Table S4. Error evaluation for filtration experiments and error analysis for the removal and rate of disappearance were carried out as described in a previous study (Nguyen et al., 2024). The measured density was determined from the mass and dimension of the support coupons with Eq. (1).

$$\rho_{\text{measured}} = \frac{m_m}{A_m h} \quad (1)$$

where  $m_m$  (g) and  $A_m = 4.91 \text{ cm}^2$  are the mass and area of the support coupon with a diameter of 2.5 cm,  $h$  (cm) is the support thickness. The porosity  $\varepsilon$  was calculated from the measured density and intrinsic density of PTFE with Eq. (2).

$$\varepsilon = \frac{\rho_m - \rho_{\text{measured}}}{\rho_m} \quad (2)$$

where  $\rho_m = 2.24 \text{ g/cm}^3$  is the intrinsic density of bulk PTFE (Quinn et al., 1951; Starkweather et al., 1982). The surface area to pore volume ( $S / V$ ) ratio was determined with Eq. (3).

$$S / V = \frac{SSA_{\text{BET}} m_m}{\varepsilon A_m h} \quad (3)$$

where  $\varepsilon A_m h$  is equal to the pore volume of the PTFE support coupon, and  $SSA_{\text{BET}}$  is the specific surface area calculated from the nitrogen gas adsorption and desorption isotherms. The  $S / V$  ratios fall in the range of  $(2.3 - 6.1) \cdot 10^5 \text{ m}^2/\text{m}^3$  for various PTFE supports in this study (Table S2).

## 2.11. Determination of the weighted average transmittance and absorbance

To compare the optical properties between the supports, the weighted average transmittance ( $T_w$ ) and absorbance ( $A_w$ ), both in percentages, were calculated for the wavelength range of 350 – 600 nm, according to Eqs. (4) and (5).

$$T_w = \frac{\int_{\lambda_{\min}}^{\lambda_{\max}} \varphi_{\text{inc},\lambda} T_\lambda d\lambda}{\int_{\lambda_{\min}}^{\lambda_{\max}} \varphi_{\text{inc},\lambda} d\lambda} \quad (4)$$

$$A_w = \frac{\int_{\lambda_{\min}}^{\lambda_{\max}} \varphi_{\text{inc},\lambda} A_\lambda d\lambda}{\int_{\lambda_{\min}}^{\lambda_{\max}} \varphi_{\text{inc},\lambda} d\lambda} \quad (5)$$

where  $\varphi_{\text{inc},\lambda}$  is the incident photon flux (photons/s.m<sup>2</sup>.nm) referenced to the AM1.5 g spectrum (ASTM, 2012; Lyubimenko et al., 2021), and  $T_\lambda$  and  $A_\lambda$  between 0 and 100 %) are the transmittance and absorbance of light at each wavelength  $\lambda$  (in nm).

## 2.12. Determination of the photon dose, singlet oxygen concentration and collision frequency

The absorbed photon flux  $\varphi_{\text{abs},V}$  (photons/L.s) was determined from the incident photon flux  $\varphi_{\text{inc},\lambda}$  (photons/s.m<sup>2</sup>.nm) and absorbance  $A_\lambda$  via Eq. (6).

$$\varphi_{\text{abs},V} = \frac{\varphi_{\text{abs},A} A_m}{V_m} = \frac{1}{h} \varphi_{\text{abs},A} = \frac{1}{h} \int_{\lambda_{\min}}^{\lambda_{\max}} \varphi_{\text{inc},\lambda} A_\lambda d\lambda \quad (6)$$

where  $\varphi_{\text{abs},A}$  (photons/m<sup>2</sup>.s) is the absorbed photon flux per effective irradiation area  $A_m$  (m<sup>2</sup>); and  $V_m$  (L) is the dimensional volume of the support. Similarly, the photon dose (or incident photon flux) per volume ( $\varphi_{\text{inc},V}$ ) can be converted from the incident photon flux per irradiated area in the wavelength range 350 – 600 nm via Eq. (7).

$$\varphi_{\text{inc},V} = \frac{1}{h} \int_{\lambda_{\min}}^{\lambda_{\max}} \varphi_{\text{inc},\lambda} d\lambda \quad (7)$$

According to theories (Baptista et al., 2017; Dumoulin, 2012) and experimental investigations (Lyubimenko et al., 2022a; Nguyen et al., 2024; Silva et al., 2010), in the absence of electron donors, porphyrins (such as PdTFPP) likely participate in a type II energy transfer process, which generates <sup>1</sup>O<sub>2</sub> as the dominant (or exclusive) ROS. The <sup>1</sup>O<sub>2</sub> concentration at the porphyrin centres was calculated according to Eq. (8) (Lyubimenko et al., 2021; Wilkinson et al., 1995), with the assumption that the drop in <sup>1</sup>O<sub>2</sub> concentration due to reaction with micropollutants (E2) is insignificant as the E2 concentration is low.

$$[{}^1\text{O}_2]_{\text{gen}} \approx \frac{\varphi_{\text{abs},V} \Phi_\Delta}{k_\Delta N_{\text{Avo}}} \quad (8)$$

where  $[{}^1\text{O}_2]_{\text{gen}}$  is the molar concentration of <sup>1</sup>O<sub>2</sub> generated at the photocatalytic centres (PdTFPP);  $\Phi_\Delta$  (no units) is the quantum yield, equal to 0.82 for <sup>1</sup>O<sub>2</sub> in coated on PTFE/PVDF supports (Lyubimenko et al., 2019);  $k_\Delta$  (s<sup>-1</sup>) is the rate constant of <sup>1</sup>O<sub>2</sub> decay, which is the inverse of the <sup>1</sup>O<sub>2</sub> lifetime; and  $N_{\text{Avo}} = 6.02 \cdot 10^{23} \text{ mol}^{-1}$  is the Avogadro constant. The uncertainty of <sup>1</sup>O<sub>2</sub> concentration was in the order of 10 %, as described in previous study (Nguyen et al., 2024).

The concentration of <sup>1</sup>O<sub>2</sub> at steady state (*i.e.* no significant diffusion under concentration gradient) as function of distance from the pore wall in radial direction was calculated from the <sup>1</sup>O<sub>2</sub> concentration at the wall as described in the previous study (Nguyen et al., 2024) and plotted in Fig. S12. In smaller (200 nm) pores, the concentration of <sup>1</sup>O<sub>2</sub> is relatively uniform in the radial direction; however, in much larger pores (in the order of 10  $\mu\text{m}$ ), the decrease in <sup>1</sup>O<sub>2</sub> concentration with increasing distance from the pore wall is more pronounced. The <sup>1</sup>O<sub>2</sub> concentration averaged for various distances from the pore surface is determined via Eq. (9).

$$[{}^1\text{O}_2]_{\text{avg}} = \frac{\int_{x_i=0}^{x_{\max}} [{}^1\text{O}_2](x_i) dx_i}{r_p} \quad (9)$$

where  $x_i$  (nm) is the distance of the <sup>1</sup>O<sub>2</sub> molecule from the pore surface; and  $x_{\max}$  (nm) is the upper limit of distance (such as the average pore radius). The collision frequency  $Z$  (mol/L.s) between <sup>1</sup>O<sub>2</sub> and steroid hormone was calculated from the respective concentrations of the reactants according to Eq. (10) (Nguyen et al., 2024; Smoluchowski, 1917).

$$Z = 4 \pi (R_{\text{O}_2} + R_{\text{E2}}) (D_{\text{O}_2} + D_{\text{E2}}) N_{\text{Avo}} [{}^1\text{O}_2]_{\text{avg}} [\text{E2}] \quad (10)$$

where  $R_{\text{O}_2} + R_{\text{E2}}$  (m) is the radius of the collision cross-section estimated as the sum of the radii of the reactants; and  $D_{\text{O}_2}$  and  $D_{\text{E2}}$  (m<sup>2</sup> s<sup>-1</sup>) are the diffusivities of <sup>1</sup>O<sub>2</sub> and E2. The effective collision frequency  $Z_{\text{eff}}$  was determined as the frequency of collisions that result in successful reactions via Eq. (11).

$$Z_{\text{eff}} = \frac{\beta}{Z} \quad (11)$$

where  $\beta$  (in %) is the steric factor, or the percentage of collisions at the suitable reactive groups to result in reaction. For the E2 – <sup>1</sup>O<sub>2</sub> pair,  $\beta$  is approximately 11 % (Nguyen et al., 2024).

The collision frequency is only an averaged value because the <sup>1</sup>O<sub>2</sub> concentration generated and, consequently, the number of collisions will decrease with increasing depth due to the following factors. Firstly, although the distribution of porphyrins on the top surface of the support is relatively even (Fig. S13), the distribution along the thickness of the support may not be uniform. In previous studies with PdTFPP-coated membranes, the distribution of PdTFPP with thickness in 130  $\mu\text{m}$  and 30  $\mu\text{m}$  thick membranes had been determined with time-of-flight secondary ion mass spectroscopy (ToF-SIMS) (Lyubimenko et al., 2019, 2022b). The ToF-SIMS results reveal that PdTFPP was more concentrated on the top and bottom surfaces of the 130  $\mu\text{m}$  thick membrane compared to the middle region (Lyubimenko et al., 2019, 2022b). For the thinner 30  $\mu\text{m}$  membrane, the PdTFPP distribution appeared more even, although PdTFPP was still found at a 67 % higher amount in the front half compared to the rear half of the membrane (Lyubimenko et al., 2022b). If these findings are linked to this study, greater concentrations of porphyrin may be found at the top and bottom of the PTFE supports. Secondly, the light intensity inside the support decreases with increasing depth due to attenuation.

## 2.13. Error analysis

The weighing of error sources in filtration experiments is the same as described in a previous study (Nguyen et al., 2024). The main contributor to feed hormone concentration error comes from the analysis (10 % uncertainty) with UHPLC-FSA. Main factors contributing to permeate hormone concentration error are: i) the analysis with UHPLC-FSA (in which the relative error increases with decreasing concentration towards the detection limit, for example, 10 % error at 100 ng/L, 10 % error at 50 ng/L, 35 % error at 10 ng/L, and 50 % error at 5 ng/L); ii) support coupon variation (around 10 % variation in permeability determined for the 0.2 mm thick coupons); and iii) variations in flux, pressure and temperature (in total 7 – 10 %). The errors in removal and rate of disappearance were propagated from the concentration errors as described by Imbrogno et al. (2024). For collision theory calculations, the relative error in <sup>1</sup>O<sub>2</sub> concentration is assumed to be around 10 % based on the porphyrin loading variation. The relative error in collision frequency is approximately 14 %, following propagation from the errors in feed steroid hormone concentration and <sup>1</sup>O<sub>2</sub> concentration. The error in specific surface area was determined from three measurement repeats per support coupon as described in the SI.

## 3. Results and discussion

The optical properties of the pristine supports and porphyrin coatings are investigated first, followed by steroid hormone removal

performance in photocatalytic filtration experiments. Photodegradation results from varying support porosity, thickness, porphyrin loading, and molar flux of steroid hormones will be correlated with calculations according to the collision theory. Lastly, the potential release of PFAS from the supports under exposure to intense UV/violet light will be examined in an accelerated aging process.

### 3.1. Light transmission through pristine ptfе porous supports

Varying the porosity and thickness of the supports can affect the light transmission through the material. This, in turn, affects the amount of light that reaches the porphyrin photosensitisers at greater depths when they are coated within the supports. Fig. 3 A – C and D provides the optical transmittance spectra of pristine (uncoated) PTFE supports for both thin supports ( $\sim 0.2$ ,  $\sim 0.3$ , and  $\sim 0.4$  mm) with four different porosities for each, along with thick supports (1 – 3 mm), each with only one porosity.

Only minimal variation in light transmittance was observed with porosity for the 0.2 mm thick supports (Fig. 3 A). Although a slight trend could be seen – transmittance increased with increasing porosity – this is more pronounced for 0.3 mm supports (Fig. 3 B) and especially for 0.4 mm supports (Fig. 3 C). Beyond a certain substrate thickness, porosity increases and reduces the number of light scattering events at the water–PTFE interfaces, resulting in better light transmission.

It appears that increasing the support thickness from 1 to 3 mm may correlate with an increasing number of scattering events and lead to an observable decrease in light transmittance at all wavelengths (Fig. 3 D). At the absorption peaks of PdTFPP, such as 518 and 550 nm (To et al., 2013) where light photons are most effectively absorbed by the immobilised PdTFPP, the transmittance decreased from 14 – 15 % with the 1 mm support to 5 – 6 % with the 3 mm support. The corresponding decrease in weighted average transmittance is from 13.5 to 5.4 % (Fig. S16 A). The pristine supports show minimal light absorption in the visible light wavelength range of 400 – 700 nm (see Fig. S14); therefore, parasitic absorption by the supports can be deemed insignificant. It is important to note that even the thickest support (3 mm) allows a small percentage (5 – 6 %) of light to transmit through at wavelengths 518 and

550 nm, which means, in theory, the PdTFPP molecules at the bottom of the support can still be irradiated and absorb light photons when these are coated within the material. However, light scattering in the PdTFPP-PTFE supports will vary from that of the pristine PTFE supports, as will be examined next.

### 3.2. Impact of porphyrin coating on the optical properties of the supports

Coating with PdTFPP may interfere with light transmission, notably due to strong light attenuation at specific wavelengths – particularly around 550, 518, and 400 nm – corresponding to the absorption peaks of PdTFPP (Lyubimenco et al., 2019; To et al., 2013). To examine light penetration, the optical transmittance spectra of the PdTFPP-PTFE supports are provided in Fig. 4 A – D.

When comparing data for coated supports (Fig. 4) with pristine supports (Fig. 3) at wavelengths  $>550$  nm, an overall reduction of transmittance caused by the coating of PdTFPP is evident. For instance, at 750 nm, light transmittance decreased from 46 – 52 to 18 – 29 % by PdTFPP coating on the 0.2 mm thick supports; similar decreases were found for all the other support thicknesses. The reduced light transmission and enhanced light scattering at the pore surface are explained by the increase in refractive index mismatch between the coated support (*i.e.* the effective medium approximation of the PdTFPP and PTFE) and water. There was a clear decreasing trend of the amount of transmitted light within the PdTFPP absorption band (300 – 550 nm) with increasing thickness. For instance, at 490 nm, light transmittance was around 4.0, 2.5, and 1.5 % for the 0.2, 0.3, and 0.4 mm supports, and  $\leq 0.1$  % for the 1 – 3 mm supports (Fig. 4 A – D). However, the transmittance at the absorption peaks of PdTFPP, such as 550, 518, and 400 nm, remained minimal at 0.01 – 0.5 %. Particularly for supports within a narrow porosity range of 30 – 35 %, the weighted average transmittance declined from 5.4 to  $<0.5$  % with increasing thickness from 0.2 to 3 mm (see Fig. S16 C). The low transmittance at the absorption peaks of PdTFPP (550, 518, and 400 nm) corresponds to the high absorbance, which exceeded 95 % and exhibited minimal variation within the fifteen PdTFPP-PTFE supports (Fig. S15). Fig. 4 A – C reveals that light transmittance appeared to vary little with support porosity for the same

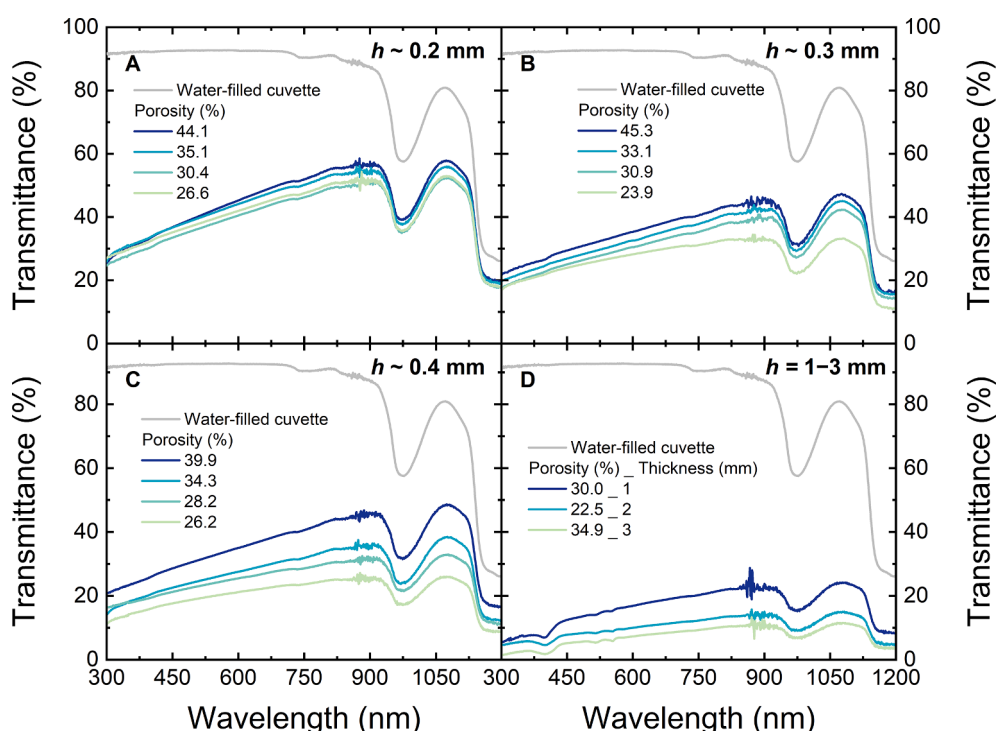


Fig. 3. Light transmittance through the pristine PTFE supports with varied approximate thicknesses  $h$  of 0.2 mm (A), 0.3 mm (B), 0.4 mm (C) and 1 – 3 mm (D).

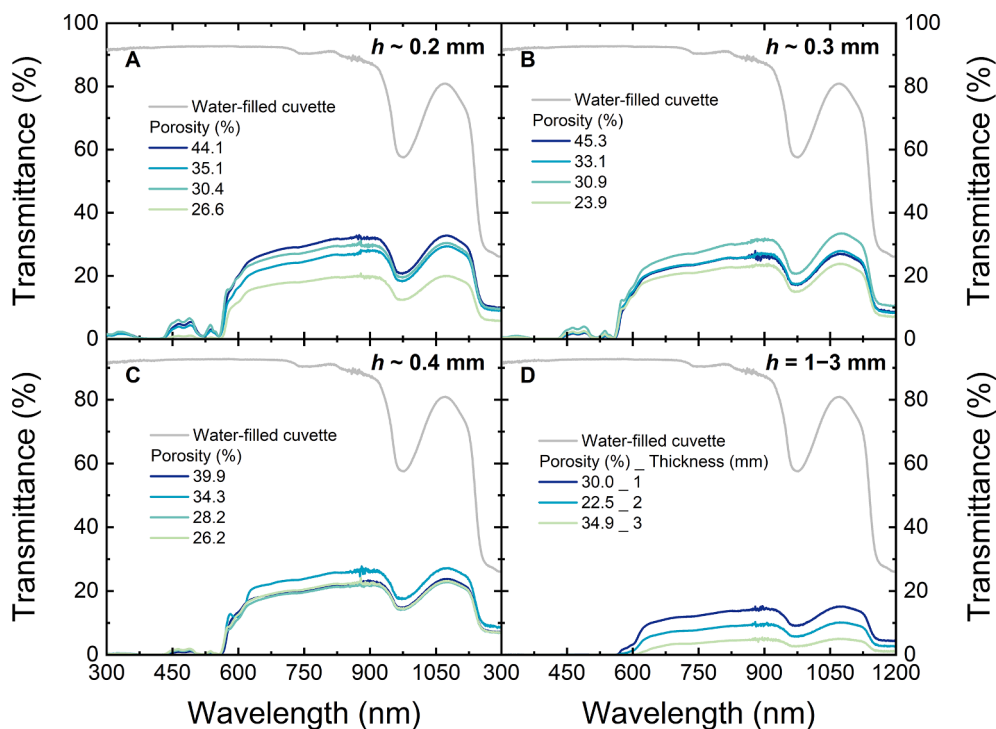


Fig. 4. Light transmittance through the porphyrin-coated PdTFPP-PTFE supports with varied approximate thicknesses  $h$  of 0.2 mm (A), 0.3 mm (B), 0.4 mm (C) and 1 – 3 mm (D).

thickness (0.2, 0.3 and 0.4 mm). According to Fig. 4 D, a small amount of light still transmitted through the thickest (3 mm) PdTFPP-PTFE support (for example, transmittance at 750 nm was 3.7 %, decreased from 9.3 % prior to PdTFPP coating). In summary, light beyond the absorption

peaks of PdTFPP can pass through a coated substrate up to 3 mm thick. However, at greater depths, the porphyrin photosensitisers may not receive enough photons within their absorption range – this is because the porphyrins at the top of the support acted as sacrificial light-

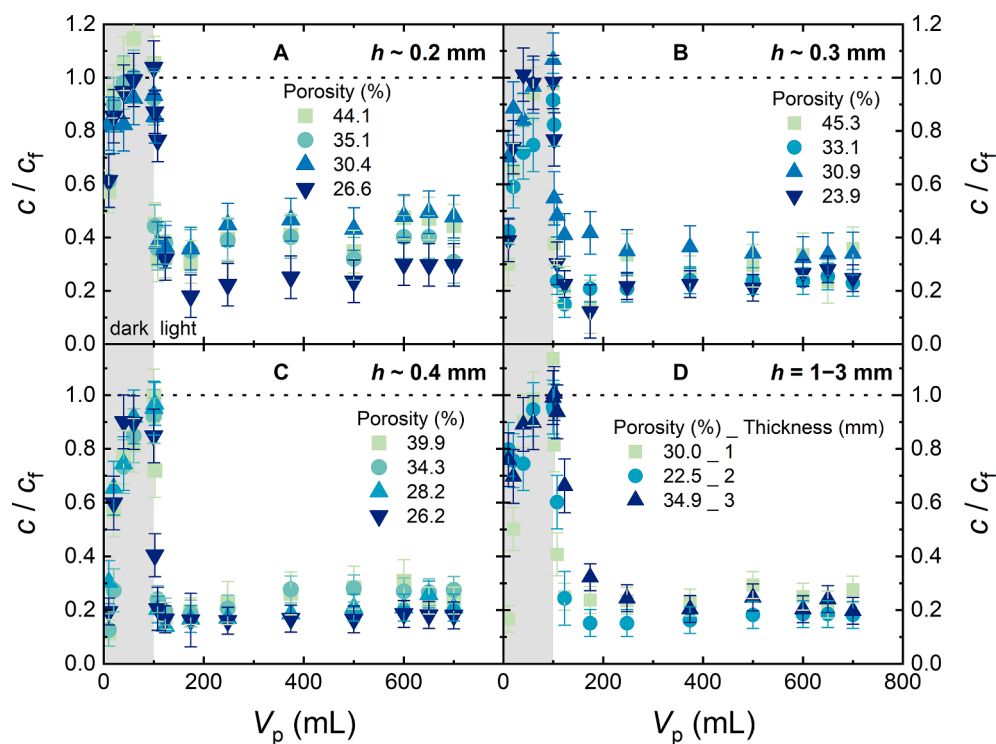


Fig. 5. Relative concentration  $c_p/c_f$  vs. permeate volume  $V_p$  with PdTFPP-PTFE supports with varied approximate thicknesses of 0.2 mm (A), 0.3 mm (B), 0.4 mm (C) and 1 – 3 mm (D) and porosities (values given in legend). PdTFPP loading 3 – 9  $\mu\text{mol/g}$ , 600  $\text{L/m}^2\cdot\text{h}$  flux,  $100 \pm 10$   $\text{ng/L}$  E2, 1 mM  $\text{NaHCO}_3$ , 10 mM  $\text{NaCl}$ , light intensity 14  $\text{mW/cm}^2$ , DO  $8.5 \pm 0.2$   $\text{mg/L}$ , pH 8,  $24.0 \pm 0.5$   $^\circ\text{C}$ . The grey area corresponds to the dark phase. Results of a pristine (uncoated) support with thickness 0.2 mm and porosity 30.4 % are shown in A to highlight minimal photodegradation without PdTFPP.

absorbing materials (Hussein et al., 2002) and suppressed the surface reflectiveness and light penetration in the support. As a result, the generation of ROS ( $^1\text{O}_2$ ) and subsequent photodegradation of steroid hormones is likely limited at increasing depths.

### 3.3. Steroid hormone removal by coated supports

The variations in light transmission and absorption among different PdTFPP-PTFE supports can lead to differing levels of photodegradation performance in photocatalytic filtration experiments. The evolution of relative concentration ( $c_p/c_f$ ) of E2, which is the ratio of the permeate concentration to the feed concentration, with permeate volume in filtration experiments is given in Fig. 5 A–D. The 0.2 – 0.4 and 1 mm thick supports were pre-saturated within 100 mL of the dark phase (Fig. S19), whereas the 2 and 3 mm thick supports required further procedure of pre-saturation (see Fig. S20 and Fig. S21 for mass balance). The experimental parameters are given in Fig. S26 and Fig. S27.

Fig. 5 A – D demonstrates that the relative concentration  $c_p/c_f$  reached an adsorption equilibrium (defined as where the permeate concentration  $c_p$  is equal to the feed concentration  $c_f$ , or  $c_p/c_f = 1$ ) at the end of the dark phase (with a permeate volume of 100 mL). When the light was switched on, the relative concentration decreased as E2 was photodegraded by all the PdTFPP-PTFE supports. The  $c_p/c_f$  results with a pristine uncoated support (thickness 0.2 mm, porosity 30.4 %) are included in Fig. 5 A to emphasise the minimal contribution of photolysis. With the coated supports, photodegradation initially disturbed the adsorption of E2 as this micropollutant was partially converted to photodegradation products (Liu et al., 2024). However, within the next 100 mL, the adsorption and desorption rates of both degraded and undegraded E2 reached equilibrium, as illustrated in Fig. S23. Within the course of the light phase (600 mL), the relative concentration eventually reached a steady state. The  $c_p/c_f$  varied between 0.50 and 0.15, which corresponds to E2 removal varying between 50 and 85 %. For a more thorough evaluation below, the supports with varied

porosities and the same thickness will be grouped (0.2, 0.3, and 0.4 mm), and any trend in steroid hormone removal within the group will be explained via the collision theory.

### 3.4. Variation of collision frequency with support porosity

For the same support thickness, the similar light transmission and absorption despite the varying support porosity (thus the  $S/V$  ratio) means that the similar quantity of useful photons had been absorbed for  $^1\text{O}_2$  generation, and this in turn will lead to similar calculated collision frequencies. To examine this, Fig. 6 shows the relative E2 concentration, E2 removal, rate of disappearance, and calculated average collision frequency at varied porosities.

From Fig. 6 A and B, the relative E2 concentration and E2 removal within the three thickness groups were independent of the porosity in the range between 22.5 and 45.3 %. When there is more pore volume in the support and a uniform feed flow rate (2 mL/min) is applied, the HRT in the pores is higher. Because the rate of disappearance is proportional to removal (which is relatively independent of porosity; see Fig. 6 B) and inversely proportional to the HRT (see Table S4), this parameter decreases with increasing porosity (Fig. 6 C). The calculated collision frequency varied only slightly with porosity (for a particular support thickness) as expected (Fig. 6 D). This means the support porosity was not a limiting factor to E2 photodegradation. It was also revealed that the collision frequency and hence the rate of reaction are lower for thicker coated supports.

In the next section, the coated supports with relatively uniform porosities and varied thicknesses from 0.2 to 3 mm will be examined to investigate whether the thickness was a limiting factor.

### 3.5. Variation of collision frequency with light penetration in the support

The PdTFPP-PTFE supports absorbed a similar amount of light in the wavelength range of 350 – 800 nm, which means that the thickness

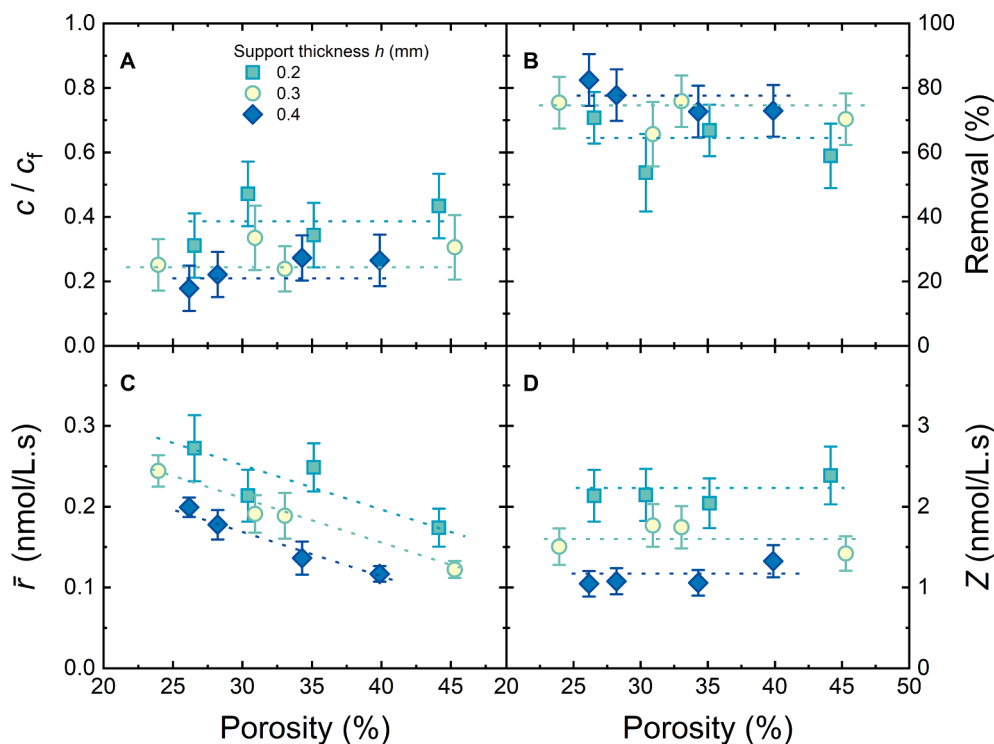


Fig. 6. Relative E2 concentration  $c/c_f$  (A), E2 removal (B), rate of disappearance  $\bar{r}$  (C) and calculated average collision frequency  $Z$  (D) with varied support porosity. PdTFPP loading 3 – 9  $\mu\text{mol/g}$ , 600  $\text{L/m}^2\cdot\text{h}$  flux,  $100 \pm 10$  ng/L E2, 1 mM  $\text{NaHCO}_3$ , 10 mM NaCl, light intensity 14  $\text{mW/cm}^2$ , DO  $8.5 \pm 0.2$  mg/L, pH 8,  $24.0 \pm 0.5$  °C.

might not be a limiting factor for  $^1\text{O}_2$  generation and E2 photodegradation, as most of the useful photons were absorbed within the 0.2 mm layer. To examine this hypothesis, the relative E2 concentration, E2 removal, rate of disappearance, and calculated average collision frequency obtained for the supports M7 – M9 and M13 – M15 are given in Fig. 7. As shown in Table S2, these supports have relatively uniform porosities ( $31 \pm 4\%$ , except the 2 mm support that has a porosity of 22.5 %).

According to Fig. 7 A and B, with the 0.2 mm thick support, the relative E2 concentration was comparably high ( $0.47 \pm 0.10$ ), corresponding to low E2 removal of ( $53 \pm 8$ ) %. E2 removal with the 0.3 mm coated support was higher at ( $66 \pm 8$ ) %. As the support thickness increased from 0.4 to 3 mm, the removal levelled off at ( $80 \pm 6$ ) %. Results imply that the photodegradation of E2 was limited by the membrane thickness in the range of 0.2 – 0.4 mm, and no longer limited in the range of 0.4 – 3 mm. Fig. 7 C shows that, when the support thickness increased from 0.2 to 0.4 mm, the rate of disappearance decreased slightly, from 0.21 to 0.18 nmol/L.s. As the support thickness increased from 0.4 to 3 mm, the rate of disappearance decreased more prominently, from 0.17 to 0.02 nmol/L.s. Because the rate of disappearance is proportional to E2 removal (which levelled off at support thicknesses between 0.4 and 3 mm) and inversely proportional to the HRT (which increases with thickness) as pointed out in Table S4, the decreasing trend means that the rate of photodegradation is not limited by the support thickness. From Fig. 7 D, the collision frequency decreased with increasing thickness. Because the concentration of  $^1\text{O}_2$  generated is proportional to the absorbance and inversely proportional to the dimensional volume of the support (see Eq. (6)), increasing the support volume (and thickness) while the light absorption varied only within a small margin reduces the average  $^1\text{O}_2$  concentration generated. If the collision frequency is multiplied by the pore volume, the resulting total amount of collisions in the whole pore space ( $Z \cdot V_{\text{pore}}$ ) increased slightly, from  $(5.8 \pm 1.2) \cdot 10^{-5}$  nmol/s with the 0.2 mm support to  $(10.1 \pm 2.0) \cdot 10^{-5}$  nmol/s with the 3 mm support (Fig. 7 D). The increase in  $Z \cdot V_{\text{pore}}$  suggests that collisions occurred at greater depths, in

spite of the reduced quantity of  $^1\text{O}_2$  generated corresponding to lower availability of useful photons, while decreasing the support thickness will likely result in poorer removal. Thinner photocatalytic layers may indeed require smaller pore sizes (*i.e.* smaller  $S/V$  ratios). In a previous study, an E2 removal of 70 % was attained with an ultra-thin (0.023 mm) PdTFPP-PTFE membrane with 200 nm diameter pores (Nguyen et al., 2024). A further enhancement in E2 removal (82 %) was reported with a similarly thin (0.03 mm) PdTFPP-PVDF membrane containing 20 nm pores under the same light intensity condition of  $14 \text{ mW/cm}^2$  (Lyubimenko et al., 2022b).

To understand the relationship between light absorption on  $^1\text{O}_2$  generation and steroid hormone photodegradation, PdTFPP loading will be investigated in the thinnest supports (0.2 mm).

### 3.6. Limitation of porphyrin loading to collision frequency

By varying the PdTFPP loading between 0.3 and  $7.7 \mu\text{mol/g}$  (see Fig. S11), the optical properties may vary, and this will affect  $^1\text{O}_2$  generation and the E2 –  $^1\text{O}_2$  collision frequency in the pores. For the assessment of these variations, the weighted average absorbance  $A_w$  and transmittance  $T_w$  for one type of coated support (thickness 0.2 mm, porosity 30.4 %) are given in Fig. 8 A. The calculated average collision frequency vs. PdTFPP loading is shown in Fig. 8 B.

From Fig. 8 A, it appears that the weighted average absorbance increases with loading. The pristine support (*i.e.* with zero loading) absorbed minimal light overall, with an  $A_w$  of only  $(2.2 \pm 0.2)\%$ .  $A_w$  increased from  $(30.1 \pm 3.0)\%$  at a loading of  $0.3 \mu\text{mol/g}$  to  $(79.4 \pm 8.0)\%$  at a loading of  $7.7 \mu\text{mol/g}$ . It is noted that the difference in optical absorption results also matches the difference in pink colour intensities observed with the naked eye (Fig. S17). The absorption spectra in Fig. S18 reveal that the absorbance at 550 and 518 nm, which are two of the absorption peaks of PdTFPP, increased from around 50 to 92 % with a loading increase from 0.3 to  $5.1 \mu\text{mol/g}$ ; at the remaining absorption peak (400 nm), light absorbance was already high ( $>89\%$ ) at the lowest loading of  $0.3 \mu\text{mol/g}$ . Fig. 8 A also reveals that the weighted

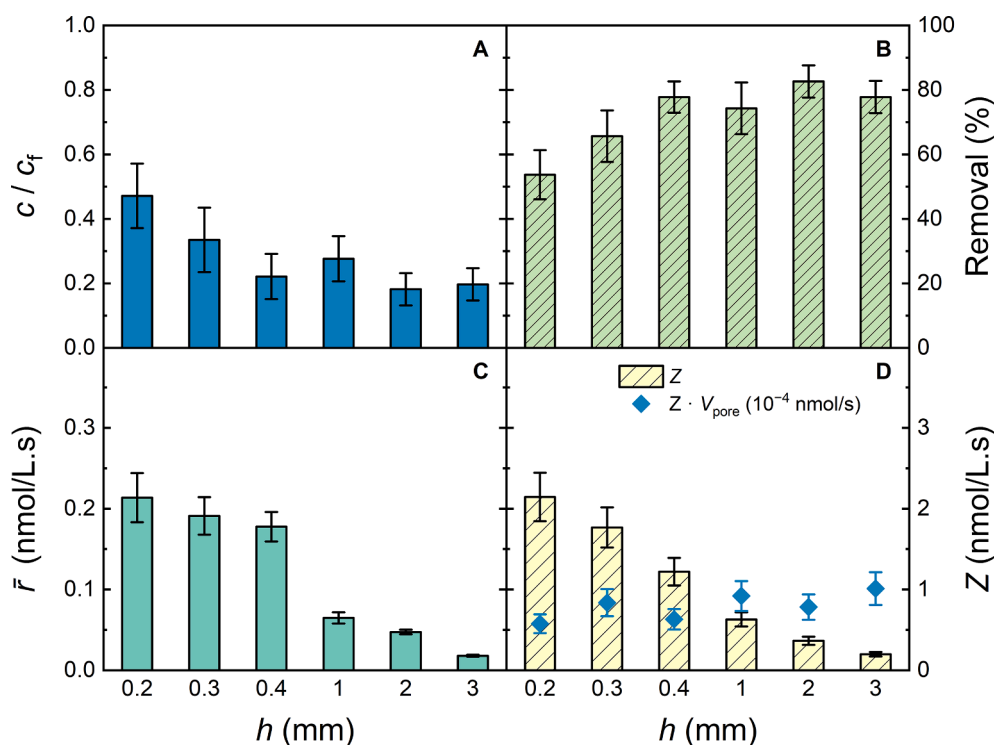
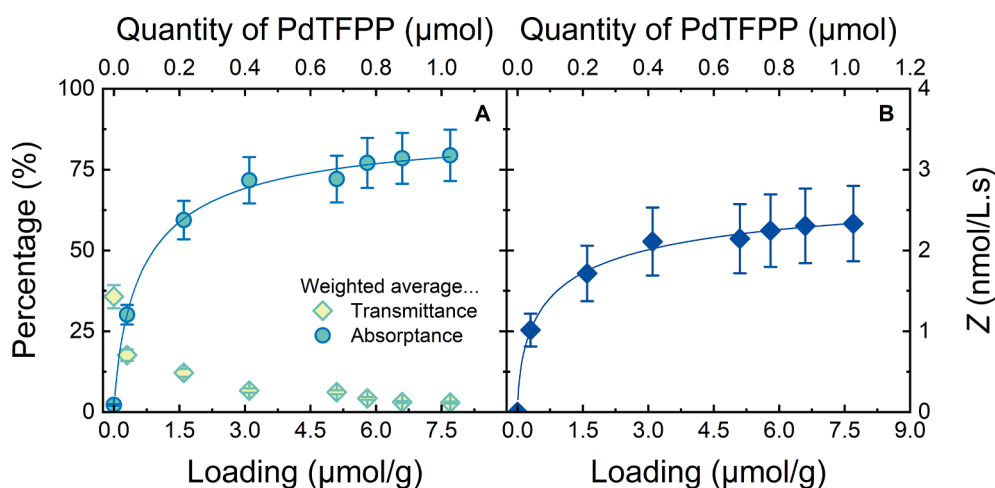


Fig. 7. Relative E2 concentration  $c/c_f$  (A), E2 removal (B), rate of disappearance  $\bar{r}$  (C) and calculated average collision frequency  $Z$  (D) vs. support thickness. PdTFPP loading 3 –  $6 \mu\text{mol/g}$ ,  $600 \text{ L/m}^2 \cdot \text{h}$  flux,  $100 \pm 10 \text{ ng/L}$  E2,  $1 \text{ mM NaHCO}_3$ ,  $10 \text{ mM NaCl}$ , light intensity  $14 \text{ mW/cm}^2$ , DO  $8.5 \pm 0.2 \text{ mg/L}$ , pH 8,  $24.0 \pm 0.5 \text{ }^\circ\text{C}$ .



**Fig. 8.** Weighted average absorbance and transmittance (A) and calculated average collision frequency  $Z$  (B) with varied PdTFPP loadings and masses of coated PdTFPP.

average transmittance  $T_w$  decreased from  $(17.6 \pm 1.8)$  to  $(2.9 \pm 0.3)$  % with an increasing loading from 0.3 to 7.7  $\mu\text{mol/g}$ . The decrease in transmittance with increasing loading (Fig. 8 A and Fig. S18 B) can be explained by the increasing mismatch between the refractive index of water and that of the support surface (which is an effective value of the combined PTFE and PdTFPP coating). According to Fig. 8 B, the calculated average collision frequency increased from 1.0 to 1.8 nmol/L.s with an increase in loading from 0.3 to 1.6  $\mu\text{mol/g}$ . Within the loading range 1.6 – 7.7  $\mu\text{mol/g}$ , this collision frequency in the pore space did not vary significantly, at around  $2.0 \pm 0.3$  nmol/L.s. The trend in collision frequency is similar to the trend in weighted average absorbance.

With only small variations in the collision frequency at loadings 1.6 – 7.7  $\mu\text{mol/g}$ , it was predicted that E2 removal would not vary significantly. To evaluate this prediction, Fig. 9 provides the relative concentration vs. permeate volume, and E2 removal and rate of disappearance vs. PdTFPP loading with the same support type (thickness 0.2 mm, porosity 30.4 %). The experimental parameters are shown in Fig. S28.

According to Fig. 9 A, in all experiments, the adsorption equilibrium was attained in the dark phase, and a steady-state concentration of E2 was reached within 600 mL of the light phase. Fig. 9 B reveals that E2 removal reached 46 % even at the lowest positive loading (0.3  $\mu\text{mol/g}$ ), and increased to 59 % with increasing loading to 1.6  $\mu\text{mol/g}$  as the

quantities of both PdTFPP and  $^1\text{O}_2$  were limited. E2 photodegradation was insignificant with the pristine support (zero PdTFPP loading). As the loading increased from 1.6 to 5.1  $\mu\text{mol/g}$ , E2 removal and rate of disappearance did not vary significantly, at  $(56 \pm 3)$  % and  $0.24 \pm 0.03$  nmol/L.s, respectively, probably because  $^1\text{O}_2$  generation was no longer limited by the quantity of PdTFPP (see Fig. 8). With a further increase in loading from 5.1 to 7.7  $\mu\text{mol/g}$ , E2 removal and rate of disappearance decreased from 54 to 23 % and from 0.22 to 0.10 nmol/L.s, respectively. This decrease in photodegradation performance could be caused by the quenching of the PdTFPP triplet state (Grenoble et al., 2005) that reduces  $^1\text{O}_2$  generation yield (Adams et al., 2019).

Specifically for the 0.2 mm thick PdTFPP-PTFE supports, a PdTFPP loading that falls between 1.6 and 5.1  $\mu\text{mol/g}$  ensures optimal photodegradation performance. The loading range may vary for other porous substrates. For example, with the ultra-thin (0.023 mm) PdTFPP-PTFE membranes with 200 nm diameter pores, the optimal loadings are between 50 and 88  $\mu\text{mol/g}$  (Nguyen et al., 2024). Because E2 removal with the optimal loadings was modest (56 %) in this study, the water flux and hence the E2 molar flux were varied in the subsequent section to investigate if there is any improvement to E2 photodegradation.

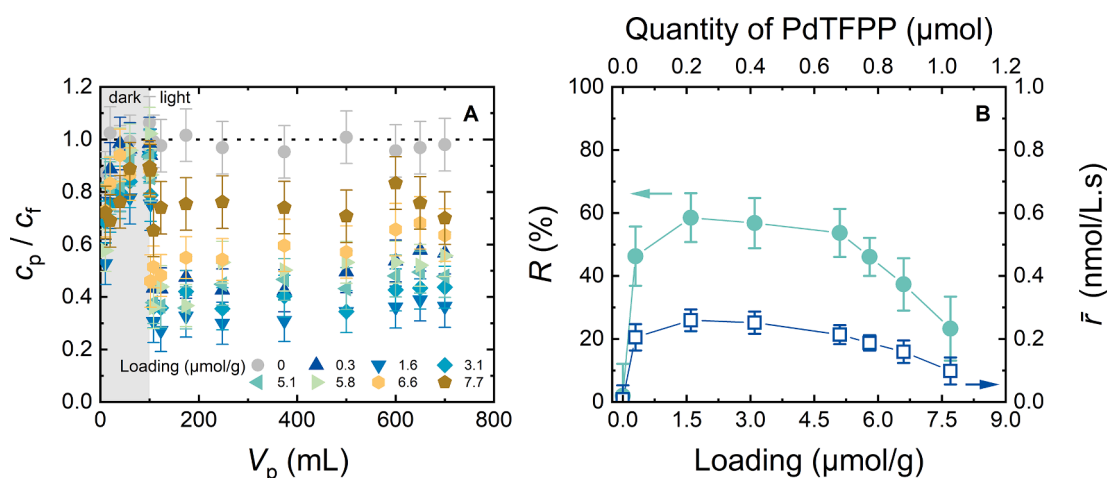


**Fig. 9.** Relative concentration  $c_p/c_f$  vs. permeate volume  $V_p$  (A), and E2 removal  $R$  and rate of disappearance  $\bar{r}$  vs. PdTFPP loading and mass of coated PdTFPP (B). Support thickness 0.2 mm and porosity 30.4 %, 600 L/m<sup>2</sup>.h flux,  $100 \pm 10$  ng/L E2, 1 mM NaHCO<sub>3</sub>, 10 mM NaCl, light intensity 14 mW/cm<sup>2</sup>, DO  $8.5 \pm 0.2$  mg/L, pH 8,  $24.0 \pm 0.5$  °C. The grey area in A corresponds to the dark phase.

### 3.7. Determination of the collision frequency threshold

If the molar flux of reactants (E2) is higher than the maximum effective collision frequency – which is around 11 % of the total collision frequency for the E2– $^1\text{O}_2$  pair (Nguyen et al., 2024) – photodegradation is limited by the E2 molar flux (and water flux). To examine how E2 removal varied with the fluxes, Fig. 10 shows the relative concentration vs. permeate volume, and E2 removal and rate of disappearance vs. water and E2 molar fluxes with the M7 supports (thickness 0.2 mm, porosity 30.4 %). The water flux was varied between 150 and 3000 L/m<sup>2</sup>.h to attain a range of E2 molar fluxes between 1.17 and 23.3 nmol/L.s, and HRTs between 3 and 0.16 s (Fig. S24). The experimental parameters are given in Fig. S29.

Steady-state was achieved within 600 mL of the light phase as permeate concentration no longer varied with increasing permeate volume (Fig. 10 A). E2 removal decreases from 79 to 26 % with water flux increasing from 300 to 3000 L/m<sup>2</sup>.h (Fig. 10 B). The rate of disappearance increased with increasing flux and appeared to reach a plateau at around 0.4 nmol/L.s. If this threshold is equal to the threshold of the effective collision frequency in the pore space  $Z_{\text{eff}}$ , i.e. the maximum collision frequency that led to reaction, the value of  $Z_{\text{eff}}$  would be approximately 0.036 nmol/L.s, representing 11 % of the total collision frequency for the E2 –  $^1\text{O}_2$  pair (Nguyen et al., 2024). Because the E2 molar flux range (1.17 and 23.3 nmol/L.s, see Fig. 10 B) is 30 – 650 times higher than  $Z_{\text{eff}}$ , it is 8 – 160 times higher than the effective collision frequency at the pore surface. As the number of collisions did not surpass the number of reactant (E2) molecules, E2 removal was always limited by the E2 molar flux (and HRT). Decreasing the fluxes will result in better photodegradation performance until the E2 molar flux is no longer a limiting factor. At that point, E2 removal will level out as observed for alternative ultra-thin PdTFPP-PTFE membranes (Nguyen et al., 2024).

It must be pointed out that at a relatively low water flux of 300 L/m<sup>2</sup>.h (equivalent to an E2 molar flux of 1.2 nmol/L.s), the E2 removal achieved by the 0.2 mm support (79 %) was similar to that achieved by a 0.023 mm PCM with a smaller pore diameter of 200 nm (74 %) (Nguyen et al., 2024) – although the limiting mechanisms are different. The smaller pores in the PCM allowed for improvement of mass transfer; however, with the thicker porous support, the reactor volume was larger and the hydraulic residence time was longer (3 s, compared to 0.6 s in the PCM). These properties allow for a higher chance of contact between E2 and the  $^1\text{O}_2$ , which partially compensated for mass transfer limitations.

### 3.8. Selectivity towards several steroid hormone types

As different steroid hormone types vary in structure, notably the presence of the aromatic ring that is susceptible to reaction with  $^1\text{O}_2$  (DeRosa and Crutchley, 2002; Lee and von Gunten, 2010), the photodegradation performance of the hormones will differ. To observe this selectivity, the relative concentration, removal, and rate of disappearance obtained with the same type of supports (thickness 0.2 mm, porosity 30.4 %) are shown in Fig. 11 for E1, E2, T, and P. Because of the strong adsorption of P by the PdTFPP-PTFE support, which resulted in the relative concentration  $c_p/c_f$  of only 0.77 within 100 mL of the dark phase, the support was pre-saturated by filtration of 700 mL feed with the light turned off (Fig. S22). The experimental parameters are shown in Fig. S30.

The relative concentration  $c_p/c_f$  for E2, T, and P approached unity within the dark phase, indicating that the supports were saturated (Fig. 11 A). For E1, the  $c_p/c_f$  ratio at the end of the dark phase was 0.85  $\pm$  0.08, which means the coupon was not yet saturated but close to saturation. In all experiments, a steady-state condition was achieved within 600 mL of the light phase. It can be observed from Fig. 11 B that the removal of E1 and E2, which contain an aromatic ring in their respective structures, was (41  $\pm$  9) and (54  $\pm$  7) %, respectively. By contrast, the removal of T and P, which contains no aromatic ring, was insignificant as the error bars were larger than the removal values. Fig. 11 B also reveals that the rates of disappearance for E1 and E2 were in the order of 0.2 nmol/L.s, while the rates of disappearance for T and P were  $\sim$ 0 nmol/L.s. It is noted that the molecular weights of these molecules vary only slightly (270 – 314 g/mol) and the frequency of total collisions between the steroid hormone and  $^1\text{O}_2$  should vary only little. It was concluded that for E1 and E2, a percentage of collisions resulted in reaction, while it seems no collisions of  $^1\text{O}_2$  with T or P resulted in reaction.

Similar observations (i.e. no removal of T and P and 50 – 76 % removal of E1 and E2) were reported for PdTFPP-PTFE membranes with smaller (200 nm) pores at the same light intensity and flux conditions (Nguyen et al., 2024). However, Lyubimenko et al. (2022b) achieved 55 % removal of T with a PdTFPP-PVDF membrane with an even smaller average pore diameter (20 nm), lower water flux (60 L/m<sup>2</sup>.h) and higher light intensity (81 mW/cm<sup>2</sup>) – the significant removal of T likely came from improved mass transfer in the small (20 nm) pores. A high activation energy would be required for  $^1\text{O}_2$  to break the olefin  $\pi$ -bond (C = C) in T and P (Frimer, 1979), whereas the activation energy would be

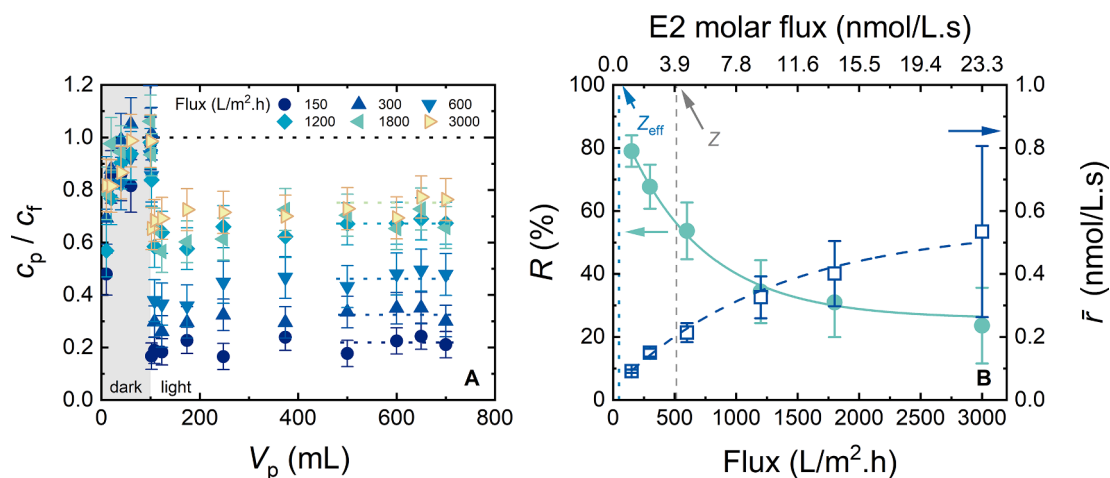


**Fig. 10.** Relative concentration  $c_p/c_f$  vs. permeate volume  $V_p$  (A), and E2 removal  $R$  and rate of disappearance  $\bar{r}$  vs. water flux and E2 molar flux (B). PdTFPP loading  $5.1 \pm 0.6$   $\mu\text{mol/g}$ , support thickness 0.2 mm and porosity 30.4 %,  $100 \pm 10$  ng/L E2, 1 mM NaHCO<sub>3</sub>, 10 mM NaCl, light intensity 14 mW/cm<sup>2</sup>, DO  $8.5 \pm 0.2$  mg/L, pH 8,  $24.0 \pm 0.5$  °C. The grey area in A corresponds to the dark phase. The trendlines in B are guides for the eye.  $Z$  and  $Z_{\text{eff}}$  in B are the total and effective collision frequencies in the pore space, respectively.

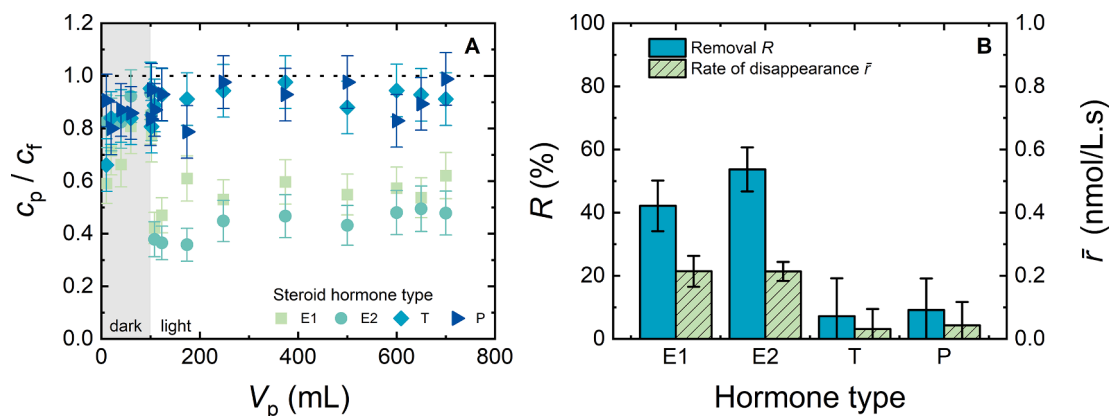


**Fig. 11.** Relative concentration  $c_p/c_f$  vs. permeate volume  $V_p$  (A), and E2 removal  $R$  and rate of disappearance  $\bar{r}$  attained with four steroid hormone types (B). PdTFPP loading  $5.1 \pm 0.6 \mu\text{mol/g}$ , support thickness 0.2 mm and porosity 30.4 %,  $100 \pm 10 \text{ ng/L}$  hormone, 1 mM  $\text{NaHCO}_3$ , 10 mM NaCl, light intensity  $14 \text{ mW/cm}^2$ , DO  $8.5 \pm 0.2 \text{ mg/L}$ , pH 8,  $24.0 \pm 0.5 \text{ }^\circ\text{C}$ . The grey area in A corresponds to the dark phase.

lower for  $^1\text{O}_2$  to react with the aromatic ring in E1 and E2 (DeRosa and Crutchley, 2002; Lee and von Gunten, 2010). This may result in reactions between  $^1\text{O}_2$  and T / P being controlled by activation instead of diffusion. The narrower pores and longer HRTs, according to Lyubimenko et al. (2022b), may allow repeated collisions between  $^1\text{O}_2$  and T, some of which can overcome the energy barrier, leading to successful reaction. The preferential reactions of  $^1\text{O}_2$  with certain micropollutant types can be exploited for selectivity.

In summary, while the thicker materials with a larger  $S / V$  ratio allowed higher porphyrin loading and deeper light penetration, neither the overall photodegradation of E2 nor the degradation of more stable steroid hormones could be improved. While the type of the ROS ( $^1\text{O}_2$ ) has not changed and thus a better removal was not to be expected, the overall degradation is most likely limited by the very large pore size (in the order of  $10 \mu\text{m}$ ), which limits the collisions between the ROS and the micropollutants to be degraded. Given the comparatively large mass of PTFE in these supports, the potential release of PFAS will then be investigated in accelerated ageing.

### 3.9. Risk of PFAS release from PTFE supports

An environmental concern of PTFE material is the risk of leaching of degradation products into the permeate during prolonged UV/violet light exposure and chemical activity of ROS. To determine whether PFAS release was significant, the concentrations of 25 different PFAS released from pristine supports with varied thicknesses (0.1 to 3 mm) and relatively uniform porosity of  $(31 \pm 4)\%$  (except the 2 mm support, 22.5 %) following accelerated aging experiments are given in Table S5. The concentrations of perfluorobutanoic acid (PFBA), perfluorohexanoic acid (PFHxA), and total PFAS are shown in Fig. 12. The coated supports were not examined because the PdTFPP was not expected to contribute to the release of PFAS from the fluoropolymer material.

After 250 h of exposure to UV/violet light, PFBA (four-carbon chain) and PFHxA (six-carbon chain), as well as total PFAS were indeed detectable in all samples. About 25 ng/L total PFAS was found in the background sample (BG, containing no PTFE supports), which would be due to background contamination. In the porous PTFE supports, the concentrations of total PFAS were higher, up to 310 ng/L. Only perfluorobutanoic (PFBA) and perfluorohexanoic acid (PFHxA) occurred at significant concentrations in all samples (Fig. 12). For the 0.2 mm supports, the total PFAS concentration (99 ng/L) was close to the regulated PFAS concentration in drinking water (European Parliament and Council, 2020). Particularly for the 0.3 mm support, the total concentration of PFAS was 310 ng/L, which is three times higher than the regulated concentration. PFAS release from the 0.4 – 3.0 mm thick

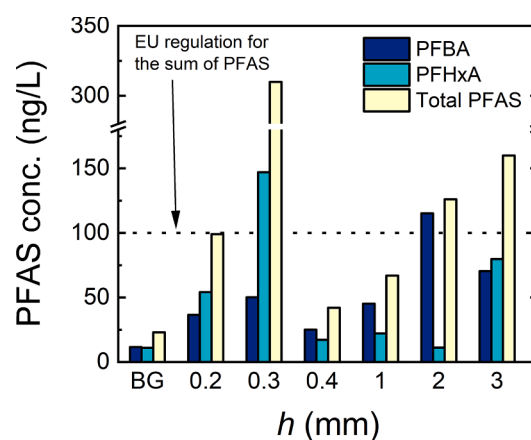


**Fig. 12.** Concentrations of two types of PFAS (perfluorobutanoic acid PFBA and perfluorohexanoic acid PFHxA), and total PFAS in the leachate solutions following accelerated aging for 250 h BG: background sample from the tray that contained no PTFE support. The horizontal dotted line indicates the limit for sum of PFAS according to the most recent EU regulation for drinking water quality.

supports appeared lower than that from the 0.3 mm support, although the total PFAS concentration increased again from 42 to 160 ng/L with a thickness increase from 0.4 to 3.0 mm. The amount of released PFAS is not solely attributed to the support mass and thickness. Other factors can affect this release, such as light penetration, positions of chain scission on the polymers (PFAS with longer chain lengths than 13 carbons were not detected), and desorption / disentanglement of PFAS molecules from the bulk material (the PFAS located deep inside the supports are less likely to be released, and longer PFAS molecules are naturally more difficult to release than shorter ones). PFAS release cannot be explained by the insignificant changes in PTFE surface chemistry. This is because the total quantity of released PFAS (0.2 – 3.0 ng per tray) is much lower, *i.e.* by nine to ten orders of magnitude, than the total mass of the PTFE coupon (140 – 2120 mg per tray, depending on the support thickness). FTIR results reveal that the surface chemistry of the PTFE support appeared unaffected by irradiation (Fig. S25). This is similar to the conclusion on the stability of poly(vinylidene fluoride) (PVDF) membranes following accelerated aging tests (Raota et al., 2023).

What does this mean? The measured values were low and staying close to the current regulation. This situation clearly represents a worst-case scenario, as the exposure to accelerated aging took place in a small volume of stagnant water. It may be the case that the limits may be further reduced, as an EU proposal suggested limiting the total PFAS in

surface water to 4.4 ng/L (European Commission, 2022b); this value is close to the detection limit for each PFAS of the standard analytical procedure (2 ng/L). Evidently, the chemical stability in accelerated ageing is limited. However, the release of PFAS shades into insignificant values if the process is applied to continuous filtration, where thousands of litres of water will be filtered through a coupon, and thus rapidly diluting the PFAS release to below picograms per litre or per hour. This is insignificant when compared to the rate of PFAS release from Teflon-coated frying pans (several nanograms per hour) (Schlummer et al., 2015). The comparisons are inevitably rough, and the precautionary principle should aim to minimise any releases, with the main concerns still fixed on the disposal of fluorinated polymers.

#### 4. Conclusions

In order to overcome limitations of thin membranes with small pores, fifteen PTFE supports with a pore size of about 10  $\mu\text{m}$ , as well as variable porosities (22.5 to 45.3 %) and thicknesses (0.2 to 3 mm) were loaded with PdTFPP porphyrin. The degradation of steroid hormone micropollutants by singlet oxygen generated by the PdTFPP porphyrin photosensitiser was quantified experimentally and theoretically using collision theory.

The surface-to-volume ( $S/V$ ) ratio of the supports falls in the range of  $10^5 - 10^6 \text{ m}^2/\text{m}^3$ , which is in the range between microreactors and photocatalytic membranes. Light transmittance differed between the pristine supports, with lower transmittance observed in less porous supports as well as the thicker supports (up to 3 mm). Porphyrin coating influenced light scattering, while the immobilised porphyrins absorbed most of the light photons at wavelengths of 550, 518, and 400 nm. Support porosity had little impact, whereas more significant variations in steroid degradation were noted with changes in the support thickness, porphyrin loading, as well as the interrelated water flux, HRT, and E2 molar flux. Process limitations were explained by the collision theory. The large pores led to a significant reduction in collision frequency due to a lack of  $^1\text{O}_2$  around the pore centre.

During accelerated aging tests under exposure to intense UV/violet light, the supports released PFAS. In all samples, the short-chained PFBA and PFHxA were found at concentrations higher than the detection limit of 10 ng/L and the background level of 25 ng/L.

While a commendable degradation of steroid hormone micropollutants was achieved with porphyrin-coated porous supports with large pores, the enhanced loading and light penetration could not achieve better results than those obtained with thin membranes.

#### CRediT authorship contribution statement

**Minh N. Nguyen:** Writing – original draft, Investigation, Visualization, Validation, Methodology, Formal analysis. **Andrey Turshatov:** Writing – review & editing, Validation, Resources, Project administration, Methodology, Funding acquisition, Formal analysis, Conceptualization. **Bryce S. Richards:** Writing – review & editing, Supervision, Resources, Methodology, Conceptualization. **Andrea I. Schäfer:** Writing – review & editing, Supervision, Resources, Methodology, Funding acquisition, Conceptualization.

#### Declaration of competing interest

The authors declare that they have no known competing financial interests or personal relationships that could have appeared to influence the work reported in this paper.

#### Acknowledgements

The German Research Foundation (DFG) is appreciated for the project funding (SOLEMBA Project, No. 500108120). The Helmholtz Association is acknowledged for providing the research infrastructure

via i) the Recruitment Initiative (A.I.S and B.S.R.); and ii) the Research Field Energy – Programme Materials and Technologies for the Energy Transition – Topic 1 Photovoltaics (38.01.05). Ministerium für Wissenschaft, Forschung und Kunst Baden-Württemberg is thanked for the funding of PFAS analyses via project Solar-driven Photocatalytic Membrane Reactors (SPheRe, 21-6221.-AFR-2/30). Berghof Fluoroplastic Technology GmbH provided the PTFE supports. Justine Nyarige (IMT, KIT) characterised the supports with SEM. Aleksandra Orlova and Eduard Madirov (IMT, KIT) are appreciated for determining the porphyrin loading and measuring the optical properties of the porous supports. Mohammad Allouzi and Camila Suliani Raota (IAMT, KIT) are thanked for the assistance with photocatalysis experiments. Siqi Liu (IAMT, KIT) provided critical comments on photocatalytic membranes and supports. Additionally, Sylwia Mozia (ZUT, Poland) is appreciated for the specific surface area characterisation, and Peter Weidler (IFG, KIT) for the discussions about errors in surface area measurements.

#### Supplementary materials

Supplementary material associated with this article can be found, in the online version, at doi:10.1016/j.watres.2024.123034.

#### Data availability

Data will be made available on request.

#### References

- Abily, M., Acuña, V., Corominas, L., Rodríguez-Roda, I., Gernjak, W., 2023. Strategic routes for wastewater treatment plant upgrades to reduce micropollutants in European surface water bodies. *J. Clean. Prod.* 415, 137867.
- Adams, M., Kozłowska, M., Baroni, N., Oldenburg, M., Ma, R., Busko, D., Turshatov, A., Emandi, G., Senge, M.O., Haldar, R., Wöll, C., Nienhaus, G.U., Richards, B.S., Howard, I.A., 2019. Highly efficient one-dimensional triplet exciton transport in a palladium–porphyrin-based surface-anchored metal–organic framework. *ACS Appl. Mater. Interfaces* 11 (17), 15688–15697.
- Alvey, J., Dev, S., Quiñones, O., Dickenson, E., Aggarwal, S., Dotson, A., 2023. Photocatalytic membrane reactor utilizing immobile photocatalytic active layer on membranes for the removal of micropollutants. *ACS. ES. T. Water* 3 (4), 1050–1059.
- Andrady, A.L., 1996. Wavelength Sensitivity in Polymer photodegradation, *Polymer Analysis Polymer Physics*. Springer, Berlin, Germany, pp. 47–94.
- Araujo, G.R., Pollmann, T., Ulrich, A., 2019. Photoluminescence response of acrylic (PMMA) and polytetrafluoroethylene (PTFE) to ultraviolet light. *Eur. Phys. J. C* 79 (8), 653–658.
- Arlos, M.J., Parker, W.J., Bicudo, J.R., Law, P., Hicks, K.A., Fuzzen, M.L.M., Andrews, S. A., Servos, M.R., 2018. Modeling the exposure of wild fish to endocrine active chemicals: potential linkages of total estrogenicity to field-observed intersex. *Water. Res.* 139, 187–197.
- ASTM, 2012. ASTM G173-03 (2012) -Standard tables for reference solar spectral irradiances: Direct normal and hemispherical on 37° tilted surface. West Conshohocken, PA.
- Baptista, M.S., Cadet, J., Di Mascio, P., Ghogare, A.A., Greer, A., Hamblin, M.R., Lorente, C., Nunez, S.C., Ribeiro, M.S., Thomas, A.H., Vignoni, M., Yoshimura, T.M., 2017. Type I and type II photosensitized oxidation reactions: guidelines and mechanistic pathways. *Photochem. Photobiol.* 93 (4), 912–919.
- Bell, E.M., De Guise, S., McCutcheon, J.R., Lei, Y., Levin, M., Li, B., Rusling, J.F., Lawrence, D.A., Cavallari, J.M., O'Connell, C., Javidi, B., Wang, X., Ryu, H., 2021. Exposure, health effects, sensing, and remediation of the emerging PFAS contaminants – Scientific challenges and potential research directions. *Sci. Total Environ.* 780, 146399.
- Bentel, M.J., Yu, Y., Xu, L., Li, Z., Wong, B.M., Men, Y., Liu, J., 2019. Defluorination of per- and polyfluoroalkyl substances (PFASs) with hydrated electrons: structural dependence and implications to PFAS remediation and management. *Environ. Sci. Technol.* 53 (7), 3718–3728.
- Berger, T.E., Regmi, C., Schäfer, A.I., Richards, B.S., 2020. Photocatalytic degradation of organic dye via atomic layer deposited TiO<sub>2</sub> on ceramic membranes in single-pass flow-through operation. *J. Membr. Sci.* 604, 118015.
- Berghof GmbH, 2024. Porous PTFE. <https://www.berghof-fluoroplastics.com/en/materials>, Accessed 23 December 2024.
- Birks, J.B., 1975. An Introduction to Liquid Scintillation Counting, and Solutes and Solvents For Liquid Scintillation Counting. Koch-Light Laboratories, Colnbrook.
- Blake, B.E., Pinney, S.M., Hines, E.P., Fenton, S.E., Ferguson, K.K., 2018. Associations between longitudinal serum perfluoroalkyl substance (PFAS) levels and measures of thyroid hormone, kidney function, and body mass index in the Fernald Community Cohort. *Environ. Pollut.* 242, 894–904.

- Bruggeman, D.A.G., 1935. Berechnung verschiedener physikalischer Konstanten von heterogenen Substanzen. I. Dielektrizitätskonstanten und Leitfähigkeiten der Mischkörper aus isotropen Substanzen. *Ann. Phys.* 416 (7), 636–664.
- Brunauer, S., Emmett, P.H., Teller, E., 1938. Adsorption of gases in multimolecular layers. *J. Am. Chem. Soc.* 60 (2), 309–319.
- Calvillo Solís, J.J., Sandoval-Pauker, C., Bai, D., Yin, S., Senftle, T.P., Villagrán, D., 2024. Electrochemical reduction of perfluorooctanoic acid (PFOA): an experimental and theoretical approach. *J. Am. Chem. Soc.* 146 (15), 10687–10698.
- Cambié, D., Bottecchia, C., Straathof, N.J.W., Hessel, V., Noël, T., 2016. Applications of continuous-flow photochemistry in organic synthesis, material science, and water treatment. *Chem. Rev.* 116 (17), 10276–10341.
- Chen, D., Li, F., Ray, A.K., 2000. Effect of mass transfer and catalyst layer thickness on photocatalytic reaction. *AIChE Journal* 46 (5), 1034–1045.
- Chen, L., Xu, P., Wang, H., 2022. Photocatalytic membrane reactors for produced water treatment and reuse: fundamentals, affecting factors, rational design, and evaluation metrics. *J. Hazard. Mater.* 424, 127493.
- Chin, S.S., Chiang, K., Fane, A.G., 2006. The stability of polymeric membranes in a TiO<sub>2</sub> photocatalysis process. *J. Membr. Sci.* 275 (1–2), 202–211.
- Ciślak, M., Kruszelnicka, I., Zembrzuska, J., Ginter-Kramarczyk, D., 2023. Estrogen pollution of the European aquatic environment: a critical review. *Water. Res.* 229, 119413.
- DeRosa, M.C., Crutchley, R.J., 2002. Photosensitized singlet oxygen and its applications. *Coord. Chem. Rev.* 233–234, 351–371.
- Dhanumalayan, E., Joshi, G.M., 2018. Performance properties and applications of polytetrafluoroethylene (PTFE) - A review. *Adv. Compos. Hybrid Mater.* 1 (2), 247–268.
- Dumoulin, F., 2012. Design and conception of photosensitizers. In: Nyokong, T., Ahsen, V. (Eds.), *Photosensitizers in Medicine, Environment, and Security*. Springer Netherlands, Dordrecht, pp. 1–46.
- European Chemicals Agency ECHA, 2023. ECHA Publishes PFAS Restriction Proposal. <https://echa.europa.eu/-/echa-publishes-pfas-restriction-proposal>. , Accessed 23 December 2024.
- European Commission, 2022a. Commission implementing Decision (EU) 2022/679 of 19 January 2022 establishing a watch list of substances and compounds of concern for water intended for human consumption as provided for in Directive (EU) 2020/2184 of the European Parliament and of the Council (notified under document C(2022) 142). <https://eur-lex.europa.eu/legal-content/EN/TXT/?uri=CELEX%3A32022D0679>, Accessed 23 December 2024.
- European Commission, 2022b. Proposal for a Directive of the European Parliament and of the Council amending Directive 2000/60/EC establishing a framework for community action in the field of water policy, Directive 2006/118/EC on the protection of groundwater against pollution and deterioration and Directive 2008/105/EC on environmental quality standards in the field of water policy. <https://eur-lex.europa.eu/legal-content/EN/TXT/?uri=CELEX%3A52022PC0540>, Accessed 23 December 2024.
- European Parliament and Council, 2020. Directive 2020/2184 of the European Parliament and of the Council of 16 December 2020 On the Quality of Water Intended For Human Consumption (recast). <https://eur-lex.europa.eu/eli/dir/2020/2184/oj>. , Accessed 23 December 2024.
- Fischer, K., Grimm, M., Meyers, J., Dietrich, C., Glaser, R., Schulze, A., 2015. Photoactive microfiltration membranes via directed synthesis of TiO<sub>2</sub> nanoparticles on the polymer surface for removal of drugs from water. *J. Membr. Sci.* 478, 49–57.
- Frimer, A.A., 1979. The reaction of singlet oxygen with olefins: the question of mechanism. *Chem. Rev.* 79 (5), 359–387.
- Gar Alalm, M., Boffito, D.C., 2022. Mechanisms and pathways of PFAS degradation by advanced oxidation and reduction processes: a critical review. *Chem. Eng. J.* 450, 138352.
- Gauch, M., Ließmann, M., Ehlers, H., Ristau, D., 2013. Optical properties of fluorocarbon thin films prepared by ion beam sputtering of PTFE. *Optical Interference Coatings. ThA.2*.
- German Institute for Standardisation, 2011. DIN 38407-42:2011-03: German Standard Methods for the Examination of Water, Waste Water and Sludge - Jointly Determinable Substances (Group F) - Part 42. <https://www.beuth.de/en/standard/din-38407-42/137282966>. , Accessed 23 December 2024.
- Gorges, R., Meyer, S., Kreisel, G., 2004. Photocatalysis in microreactors. *J. Photochem. Photobiol. A: Chem.* 167 (2), 95–99.
- Grenoble, S., Gouterman, M., Khalil, G., Callis, J., Dalton, L., 2005. Pressure-sensitive paint (PSP): concentration quenching of platinum and magnesium porphyrin dyes in polymeric films. *J. Lumin.* 113 (1), 33–44.
- Guo, Q., Huang, Y., Xu, M., Huang, Q., Cheng, J., Yu, S., Zhang, Y., Xiao, C., 2022. PTFE porous membrane technology: a comprehensive review. *J. Membr. Sci.* 664, 121115.
- Han, X., Shen, J., Yin, P., Hu, S., Bi, D., 2014. Influences of refractive index on forward light scattering. *Opt. Commun.* 316, 198–205.
- Hodges, B.C., Cates, E.L., Kim, J.-H., 2018. Challenges and prospects of advanced oxidation water treatment processes using catalytic nanomaterials. *Nat. Nanotechnol.* 13 (8), 642–650.
- Huang, Q.-L., Xiao, C.-f., Feng, X.-s., Hu, X.-Y., 2013. Design of super-hydrophobic microporous polytetrafluoroethylene membranes. *New J. Chem.* 37 (2), 373–379.
- Huang, Q., Xiao, C., Hu, X., 2012. Preparation and properties of polytetrafluoroethylene/CaCO<sub>3</sub> hybrid hollow fiber membranes. *J. Appl. Polym. Sci.* 123 (1), 324–330.
- Hussein, M.A., Sivakumar, S., Corp, I., 2002. US6365529B1 Patent - Method For Patterning Dual Damascene Interconnects Using a Sacrificial Light Absorbing Material. USA.
- Imbrogno, A., Nguyen, M.N., Schäfer, A.I., 2024. Tutorial review of error evaluation in experimental water research at the example of membrane filtration. *Chemosphere* 357, 141833.
- Joers, H., Menger, F., Tang, J., Ebinghaus, R., Ahrens, L., 2022. Beyond the tip of the iceberg: suspect screening reveals point source-specific patterns of emerging and novel per- and polyfluoroalkyl substances in German and Chinese Rivers. *Environ. Sci. Technol.* 56 (9), 5456–5465.
- Johnson, A.C., Jin, X., Nakada, N., Sumpter, J.P., 2020. Learning from the past and considering the future of chemicals in the environment. *Science* 367 (6476), 384–387.
- Kumari, P., Bahadur, N., Dumée, L.F., 2020. Photo-catalytic membrane reactors for the remediation of persistent organic pollutants – A review. *Sep. Purif. Technol.* 230, 115878.
- Kvalem, H.E., Nygaard, U.C., Lødrup Carlsen, K.C., Carlsen, K.H., Haug, L.S., Granum, B., 2020. Perfluoroalkyl substances, airways infections, allergy and asthma related health outcomes – implications of gender, exposure period and study design. *Environ. Int.* 134, 105259.
- Lauretta, R., Sansone, A., Sansone, M., Romanelli, F., Appetecchia, M., 2019. Endocrine disrupting chemicals: effects on endocrine glands. *Front. Endocrinol. (Lausanne)* 10, 436971.
- Lee, Y., von Gunten, U., 2010. Oxidative transformation of micropollutants during municipal wastewater treatment: comparison of kinetic aspects of selective (chlorine, chlorine dioxide, ferrate<sup>VI</sup>, and ozone) and non-selective oxidants (hydroxyl radical). *Water. Res.* 44 (2), 555–566.
- Li, L., Tang, D., Song, Y., Jiang, B., 2018. Dual-film optofluidic microreactor with enhanced light-harvesting for photocatalytic applications. *Chem. Eng. J.* 339, 71–77.
- Liu, S., Jassby, D., Mandler, D., Schäfer, A.I., 2024. Differentiation of adsorption and degradation in steroid hormone micropollutants removal using electrochemical carbon nanotube membrane. *Nat. Commun.* 15, 9524.
- Lockwood, D.J., 2016. Rayleigh and Mie scattering. In: Luo, M.R. (Ed.), *Encyclopedia of Color Science and Technology*. Springer New York, New York, NY, pp. 1097–1107.
- Ly, Q.V., Cui, L., Asif, M.B., Khan, W., Nghiem, L.D., Hwang, Y., Zhang, Z., 2023. Membrane-based nanoconfined heterogeneous catalysis for water purification: a critical review. *Water. Res.* 230, 119577.
- Lyubimenko, R., Busko, D., Richards, B.S., Schäfer, A.I., Turshatov, A., 2019. Efficient photocatalytic removal of methylene blue using a metalloporphyrin–poly(vinylidene fluoride) hybrid membrane in a flow-through reactor. *ACS Appl. Mater. Interfaces* 11 (35), 31763–31776.
- Lyubimenko, R., Gutierrez Cardenas, O.I., Turshatov, A., Richards, B.S., Schäfer, A.I., 2021. Photodegradation of steroid-hormone micropollutants in a flow-through membrane reactor coated with Pd(II)-porphyrin. *Appl. Catal. B: Environ.* 291, 120097.
- Lyubimenko, R., Richards, B.S., Schäfer, A.I., Turshatov, A., 2022a. Noble-metal-free photosensitizers for continuous-flow photochemical oxidation of steroid hormone micropollutants under sunlight. *J. Membr. Sci.* 642, 119981.
- Lyubimenko, R., Richards, B.S., Turshatov, A., Schäfer, A.I., 2020. Separation and degradation detection of nanogram-per-litre concentrations of radiolabelled steroid hormones using combined liquid chromatography and flow scintillation analysis. *Sci. Rep.* 10 (1), 7095.
- Lyubimenko, R., Turshatov, A., Welle, A., Weidler, P.G., Richards, B.S., Schäfer, A.I., 2022b. Enhanced photocatalytic efficiency via improved contact in a solar-driven membrane reactor for steroid hormone removal. *Chem. Eng. J.* 138449.
- Morisue, M., Kawanishi, M., Miyake, Y., Kanaori, K., Tachibana, K., Ohke, M., Kohri, M., Matsui, J., Hoshino, T., Sasaki, S., 2023. Metallic lustrous porphyrin foil with an exceptional refractive index. *Macromolecules.* 56 (19), 7993–8002.
- Moza, S., 2010. Photocatalytic membrane reactors (PMRs) in water and wastewater treatment. A review. *Sep. Purif. Technol.* 73 (2), 71–91.
- Newton, S., McMahan, R., Stoeckel, J.A., Chislock, M., Lindstrom, A., Strynar, M., 2017. Novel polyfluorinated compounds identified using high resolution mass spectrometry downstream of manufacturing facilities near Decatur, Alabama. *Environ. Sci. Technol.* 51 (3), 1544–1552.
- Nguyen, M.N., Raota, C.S., Turshatov, A., Richards, B.S., Schäfer, A.I., 2024. Collision theory and membrane photocatalysis: steroid hormones meet singlet oxygen in palladium-porphyrin-coated polytetrafluoroethylene membranes. *Chem. Eng. J.* 501, 127582.
- Nowack, E.C.M., Podola, B., Melkonian, M., 2005. The 96-well twin-layer system: a novel approach in the cultivation of microalgae. *Protist.* 156 (2), 239–251.
- Nyamutswa, L.T., Zhu, B., Collins, S.F., Navaratna, D., Duke, M.C., 2020. Light conducting photocatalytic membrane for chemical-free fouling control in water treatment. *J. Membr. Sci.* 604, 118018.
- Orozco-Hernández, L., Gómez-Oliván, L.M., Elizalde-Velázquez, A., Natividad, R., Fabian-Castoño, L., SanJuan-Reyes, N., 2019. 17-β-Estradiol: significant reduction of its toxicity in water treated by photocatalysis. *Sci. Total Environ.* 669, 955–963.
- Penttilä, A., Lumme, K., 2009. The effect of the properties of porous media on light scattering. *J. Quant. Spectrosc. Radiat. Transfer* 110 (18), 1993–2001.
- Pétre, M.A., Salk, K.R., Stapleton, H.M., Ferguson, P.L., Tait, G., Obenour, D.R., Knappe, D.R.U., Genereux, D.P., 2022. Per- and polyfluoroalkyl substances (PFAS) in river discharge: modeling loads upstream and downstream of a PFAS manufacturing plant in the Cape Fear watershed. North Carolina. *Sci. Total Environ.* 831, 154763.
- Qin, Y., Jian, S., Bai, K., Wang, Y., Mai, Z., Fan, S., Qiu, B., Chen, Y., Wang, Y., Xiao, Z., 2020. Catalytic membrane reactor of nano (Ag+ZIF-8)/poly(tetrafluoroethylene) built by deep-permeation synthesis fabrication. *Ind. Eng. Chem. Res.* 59 (21), 9890–9899.
- Qing, W., Liu, F., Yao, H., Sun, S., Chen, C., Zhang, W., 2020. Functional catalytic membrane development: a review of catalyst coating techniques. *Adv. Colloid. Interface Sci.* 282, 102207.
- Quill, T., Weiss, S., Hirschler, C., Pankadz, V., DiBattista, G., Arthur, M., Chen, J., 2020. Ultraviolet reflectance of microporous PTFE. <https://www.porex.com/wp-content/>

- uploads/2020/04/Ultraviolet-Reflectance-of-Microporous-PTFE.pdf. , Accessed 23 December 2024.
- Quinn, F.A., Roberts, D.E., Work, R.N., 1951. Volume-temperature relationships for the room temperature transition in teflon. *J. Appl. Phys.* 22 (8), 1085–1086.
- Ramirez-Cuevas, F.V., Gurunatha, K.L., Parkin, I.P., Papakonstantinou, I., 2022. Universal theory of light scattering of randomly oriented particles: a fluctuational-electrodynamics approach for light transport modeling in disordered nanostructures. *ACS. Photonics.* 9 (2), 672–681.
- Raota, C.S., Lotfi, S., Lyubimenko, R., Richards, B.S., Schäfer, A.I., 2023. Accelerated ageing method for the determination of photostability of polymer-based photocatalytic membranes. *J. Membr. Sci.* 686, 121944.
- Regmi, C., Lotfi, S., Espíndola, J.C., Fischer, K., Schulze, A., Schäfer, A.I., 2020. Comparison of photocatalytic membrane reactor types for the degradation of an organic molecule by TiO<sub>2</sub>-coated PES membrane. *Catalysts.* 10 (7), 725.
- Ren, Z., Bergmann, U., Leiviskä, T., 2021. Reductive degradation of perfluorooctanoic acid in complex water matrices by using the UV/sulfite process. *Water. Res.* 205, 117676.
- Richards, B.S., 2004. Comparison of TiO<sub>2</sub> and other dielectric coatings for buried-contact solar cells: a review. *Prog. Photovolt.: Res. Appl.* 12 (4), 253–281.
- Schlummer, M., Sölch, C., Meisel, T., Still, M., Gruber, L., Wolz, G., 2015. Emission of perfluoroalkyl carboxylic acids (PFCA) from heated surfaces made of polytetrafluoroethylene (PTFE) applied in food contact materials and consumer products. *Chemosphere* 129, 46–53.
- Silva, E.F.F., Serpa, C., Dąbrowski, J.M., Monteiro, C.J.P., Formosinho, S.J., Stochel, G., Urbanska, K., Simões, S., Pereira, M.M., Arnaut, L.G., 2010. Mechanisms of singlet-oxygen and superoxide-ion generation by porphyrins and bacteriochlorins and their implications in photodynamic therapy. *Chem. – Eur. J.* 16 (30), 9273–9286.
- Singh, B., Sharma, N., 2008. Mechanistic implications of plastic degradation. *Polym. Degrad. Stab.* 93 (3), 561–584.
- Skovsen, E., Snyder, J.W., Lambert, J.D.C., Ogilby, P.R., 2005. Lifetime and diffusion of singlet oxygen in a cell. *J. Phys. Chem. B* 109 (18), 8570–8573.
- Smoluchowski, M.v., 1917. Versuch einer mathematischen Theorie der Koagulationskinetik kolloider Lösungen. *Z. Phys. Chem.* 92 (1), 129–168.
- Starkweather, H.W., Zoller, P., Jones, G.A., Vega, A.J., 1982. The heat of fusion of polytetrafluoroethylene. *J. Polym. Sci.* 20 (4), 751–761.
- Su, R., Zhu, Y., Gao, B., Li, Q., 2024. Progress on mechanism and efficacy of heterogeneous photocatalysis coupled oxidant activation as an advanced oxidation process for water decontamination. *Water. Res.* 251, 121119.
- Su, Y., Straathof, N.J.W., Hessel, V., Noël, T., 2014. Photochemical transformations accelerated in continuous-flow reactors: basic concepts and applications. *Chem. – Eur. J.* 20 (34), 10562–10589.
- Tagliavini, M., Engel, F., Weidler, P.G., Scherer, T., Schäfer, A.I., 2017. Adsorption of steroid micropollutants on polymer-based spherical activated carbon (PBSAC). *J. Hazard. Mater.* 337, 126–137.
- Tang, M., Wan, J., Wang, Y., Ye, G., Yan, Z., Ma, Y., Sun, J., 2024. Overlooked role of void-nanoconfined effect in emerging pollutant degradation: modulating the electronic structure of active sites to accelerate catalytic oxidation. *Water. Res.* 249, 120950.
- Tang, Z., Liu, Z.-h., Wang, H., Dang, Z., Yin, H., Zhou, Y., Liu, Y., 2020. Trace determination of eleven natural estrogens and insights from their occurrence in a municipal wastewater treatment plant and river water. *Water. Res.* 182, 115976.
- Thiruraman, J.P., Masih Das, P., Drndić, M., 2020. Ions and water dancing through atom-scale holes: a perspective toward “size zero. *ACS. Nano* 14 (4), 3736–3746.
- To, W.-P., Liu, Y., Lau, T.-C., Che, C.-M., 2013. A robust palladium(II)–porphyrin complex as catalyst for visible light induced oxidative C–H functionalization. *Chem. – Eur. J.* 19 (18), 5654–5664.
- Tran, N.H., Reinhard, M., Gin, K.Y.-H., 2018. Occurrence and fate of emerging contaminants in municipal wastewater treatment plants from different geographical regions - A review. *Water. Res.* 133, 182–207.
- United Nations, 2017. **United Nations World Water Development Report, Wastewater: The untapped Resource.** <https://www.unep.org/resources/publication/2017-un-world-water-development-report-wastewater-untapped-resource>. , Accessed 23 December 2024.
- Vandenberg, L.N., Colborn, T., Hayes, T.B., Heindel, J.J., Jacobs, D.R., Lee, D.-H., Shioda, T., Soto, A.M., vom Saal, F.S., Welshons, W.V., Zoeller, R.T., Myers, J.P., 2012. Hormones and endocrine-disrupting chemicals: low-dose effects and nonmonotonic dose responses. *Endocr. Rev.* 33 (3), 378–455.
- Wang, R., Ma, X., Liu, T., Li, Y., Song, L., Tjong, S.C., Cao, L., Wang, W., Yu, Q., Wang, Z., 2020. Degradation aspects of endocrine disrupting chemicals: a review on photocatalytic processes and photocatalysts. *Appl. Catal. A: Gen.* 597, 117547.
- Wielsoe, M., Long, M., Ghisari, M., Bonefeld-Jørgensen, E.C., 2015. Perfluoroalkylated substances (PFAS) affect oxidative stress biomarkers in vitro. *Chemosphere* 129, 239–245.
- Wilkinson, F., Helman, W.P., Ross, A.B., 1995. Rate constants for the decay and reactions of the lowest electronically excited singlet state of molecular oxygen in solution. An expanded and revised compilation. *J. Phys. Chem. Ref. Data* 24 (2), 663–677.
- Xin, X., Kim, J., Ashley, D.C., Huang, C.-H., 2023. Degradation and defluorination of per- and polyfluoroalkyl substances by direct photolysis at 222 nm. *ACS. ES. T. Water.* 3 (8), 2776–2785.
- Yang, Y., Zhang, X., Jiang, J., Han, J., Li, W., Li, X., Yee Leung, K.M., Snyder, S.A., Alvarez, P.J.J., 2022. Which micropollutants in water environments deserve more attention globally? *Environ. Sci. Technol.* 56 (1), 13–29.
- Yu, S., Chen, J., Gomard, G., Hölscher, H., Lemmer, U., 2023. Recent progress in light-scattering porous polymers and their applications. *Adv. Opt. Mater.* 11 (13), 2203134.